Accepted Manuscript

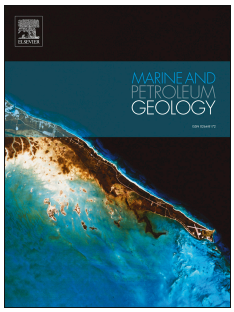

Styles of basal interaction beneath mass transport deposits

Matheus S. Sobiesiak, Ben Kneller, G. Ian Alsop, JuanPablo Milana

PII: S0264-8172(18)30352-0

DOI: 10.1016/j.marpetgeo.2018.08.028

Reference: JMPG 3468

To appear in: *Marine and Petroleum Geology*

Received Date: 24 August 2017

Revised Date: 20 August 2018

Accepted Date: 23 August 2018

Please cite this article as: Sobiesiak, M.S., Kneller, B., Alsop, G.I., Milana, J., Styles of basal interaction beneath mass transport deposits, *Marine and Petroleum Geology* (2018), doi: 10.1016/j.marpetgeo.2018.08.028.

Styles of basal interaction beneath mass transport deposits

Matheus. S. Sobiesiak[1,3], Ben Kneller[1], G. Ian Alsop[1], Juan.Pablo. Milana[2]

[1] Dept. of Geology and Petroleum Geology, University of Aberdeen, Aberdeen AB24 3UE, Scotland, U.K.
[2] Universidad Nacional de San Juan, Mitre Este, San Juan, Argentina
[3] Present address: Programa de Pós-graduação em Geologia, Universidade do Vale do Rio dos Sinos, 93022-000, São Leopoldo, Rio Grande do Sul, Brazil.

Corresponding author.
E-mail addresses: matheus.sobiesiak@gmail.com (M.S.Sobiesiak), b.kneller@abdn.ac.uk (B.Kneller), ian.alsop@abdn.ac.uk (G.I.Alsop), jpmilana@gmail.com (J.P.Milana).

1 Abstract

Erosion of the seafloor is often interpreted to be the result of turbidity currents and reflects their frictional and non-cohesive nature. However, evidence of the interaction between sediment gravity-flows and the substrate forming the sea floor has been increasingly reported in the literature. Based on styles of basal interaction with the substrate, we here propose a broad classification of submarine mass movements labelled free- and no-slip flows. Three mechanisms are proposed for free-slip flows during translation of mass movements that are effectively detached from the substrate; hydroplaning, shear wetting, and substrate liquefaction. In contrast, no-slip flows occur where the mass movement is welded to the substrate, and the strain front lies within the substrate itself. In the latter case, flows can erode by pushing forward and/or ploughing into the substrate, often remobilizing sediments that are later incorporated into the flow, a common characteristic shared by many mass transport deposits (MTDs) containing blocks. Additionally, linear track features (e.g. grooves and striations) are described as a consequence of substrate tooling by rigid blocks. Using outcrops in NW Argentina as a detailed case study, we have recorded evidence for penetration of the strain profile into sediments underlying MTDs and categorised the deformation into no-slip basal deformation that may display continuous and discontinuous profiles. Continuous deformation profiles involve the complete deformation of the uppermost layers of the substrate, while discontinuous deformation profiles preserve a undeformed substrate layer between the MTD and the zone of deformed substrate. These features highlight the erosive and deformational nature of MTDs, and can be used as potential kinematic indicators.

2 Introduction

Sediment failure on a slope occurs in response to gravitational forces with or without the additional effects of seismicity (e.g. Dott, 1963; Hampton et al., 1996; Middleton and Hampton, 1973; Moscardelli and Wood, 2008; Nardin et al., 1979). The resulting mass flows are highly mobile and lead to sediments being transferred from regions of higher gradient (e.g. shelf break and upper slope) onto lower gradients (e.g. deep-water) through downslope translation over a basal shear surface. Mass flows can range in volume from tens of cubic metres (~2 x 10^{-4} km^3) up to hundreds of thousands of cubic kilometres (~ 259 x 10^3 km^3), extend over an area of tens of millions of square kilometres (~ 114 x 10^5 km^2) (e.g. Denne et al., 2013; Moscardelli and Wood, 2015), and have long run-out distance (400 kilometres) over very low-angled (0.05°) slopes (Gee et al., 1999). Such processes are highly complex, and the resulting deposits, normally termed mass transport deposits (MTDs) or complexes (MTCs), are highly variable in their geometry, composition and degree of internal deformation, depending on the geological setting and many other factors. They include deposits described as slides, slumps and debris flows (Moscardelli and Wood, 2008). In addition, they may have a significant impact on their surroundings either by modifying previously deposited sedimentary sequences, or by creating topography, which subsequently controls the pathway of turbidity currents (Kneller et al., 2016).

MTDs can be classified as frontally confined or frontally emergent according to their frontal emplacement (**Fig 1**) (Frey-Martínez et al., 2006). Frontally confined MTDs occur when the flow undergoes relatively limited downslope movement and does not have enough momentum to overcome the frontal ramp and translate over the sea floor. This results in the flow being restricted to the area directly overlying the basal shear surface (BSS) that separates the MTD from undeformed strata, both older than (beneath) and stratigraphically equivalent to(downslope) those involved in the MTD (Frey-Martínez et al., 2006). Conversely, frontally emergent MTDs occur when the flow is able to overrun its frontal ramp, extending beyond its original BSS, and is free to flow over the seafloor (Frey-Martínez et al., 2006).

The potentially interactive character of the basal contact of MTDs was documented in early works by Prior et al., (1984), where a frontally emergent debris flow was described as possessing an “eroding base” that could incorporate a considerable amount of sea floor material. Additionally linear features (termed glide tracks) were created by detached masses

of sediment that moved beyond the main flow deposit over undeformed sea floor (Prior et al., 1984). A large number of subsequent publications have used seismic datasets to illustrate basal erosion, including features such as scours (Nissen et al., 1999; Posamentier and Kolla, 2003), glide tracks (Nissen et al., 1999; Prior et al., 1984), grooves (Bull et al., 2009; Posamentier and Kolla, 2003), striations (Bull et al., 2009; Gee et al., 2005), ramp and flat systems (Bull et al., 2009; Omosanya and Alves, 2013), megascours (Moscardelli et al., 2006) and features that splay in plan view, variously described as cat claws (Moscardelli et al., 2006), and monkey fingers (McGilvery and Cook, 2003), among others.

The basal interaction of MTDs with the underlying substrate is widely documented from seismic data (e.g. Alves et al., 2013; Bull et al., 2009; Gee et al., 2005; McGilvery and Cook, 2003; Moscardelli et al., 2006; Omosanya and Alves, 2013; Posamentier and Martinsen, 2011) and more rarely in outcrop (e.g. Butler and Tavarnelli, 2006; Dakin et al., 2013; Dykstra et al., 2011; Gawthorpe and Clemmey, 1985; Lucente and Pini, 2003; Ogata et al., 2012; Sobiesiak et al., 2016a), but the nature of this interaction with the substrate is poorly understood. In this paper, we propose two styles of basal interaction broadly classified as; (i) free-slip flow; and (ii) no-slip flow (**Fig 2**). To illustrate the basal contact and the interaction with the underlying substrate, we present examples from a variety of previously published and original case studies.

3 Styles of basal interaction

3.1 Free-slip flows

A mass flows may override the substrate with little or no sign of its passage preserved in the strata below the basal shear surface (**Fig 2a and b**). This implies no significant interaction such as erosion and deformation, although minor interaction may develop such as mobilization and/or mixing between the flow and the underlying deposits, especially during deposition.

3.1.1 Hydroplaning

Laboratory experiments and theoretical models often compare submarine debris flows with their subaerial counterparts to better understand the flow mechanics and physical properties (e.g. Mohrig et al., 1999; Toniolo et al., 2004). Some of these experiments suggest a flow mechanism termed hydroplaning to explain why some submarine debris flow are apparently more mobile and have longer runout distances than their subaerial equivalents

(Ilstad et al., 2004a; Mohrig et al., 1999, 1998). Hydroplaning is considered to develop when the hydrodynamic water pressure at the front of the flow increases and is transferred down from the front of the flow into the underlying bed (Mohrig et al., 1998). The overburden pressure at the base of the flow enables the penetration of a discrete water layer that separates the flow from the underlying bed (De Blasio and Elverhøi, 2011; Mohrig et al., 1998) (**Fig 2a**). The lubricating layer of water-rich sediment below the debris flow has a lower viscosity than either the debris flow or the underlying substrate and is therefore easily sheared. Where only the head of the flow is hydroplaning, it accelerates away from the (non-hydroplaning) body due to substantially lower basal resistance, causing the region immediately behind the head to extend and attenuate (stretching zone) in a process referred to as necking (Mohrig et al., 1998). The stretching zone behind the head is prone to interact with water from the lubricant layer, that is progressively transformed into a muddier layer. In turn, small cracks are developed at the base of the flow, due to the increased pore pressure and consequently reduction of effective stresses produced by the water diffusion at the flow base (Ilstad et al., 2004b). If the flow experiences further translation, it can cause the complete detachment of the hydroplaning head (auto-acephalation), resulting in a secondary head and an 'outrunner block' comprised by the detached head (Ilstad et al., 2004a; Mohrig et al., 1998). The basal shear stress produced by the translation of the flow is not transferred into the substrate via the lubricant layer due to the large difference in viscosity (Mohrig et al., 1999).

3.1.2 Shear wetting

Another explanation for the lack of interaction between the debris flow and the substrate deposits is the 'shear wetting model' (De Blasio et al., 2005). Shear wetting results from high shear rates established between the water and sediment boundary during flow, leading to dilution of the base of the flow and a significant decrease in shear strength (**Fig 2a**). On the other hand, the entrainment of small amounts of clay into the lubricant layer will greatly increase its yield stress and viscosity when compared to pure water, while still being lower than the overlying flow (Ilstad et al., 2004b). This process creates a softer, more dilute phase (slurry) that acts as a lubricating layer (De Blasio and Elverhøi, 2011; De Blasio et al., 2005). Shear wetting can also be achieved during hydroplaning when cracks in the necking region enable the penetration of water into the base of the flow, resulting in the development of a lubricating slurry layer (Elverhøi et al., 2005; Ilstad et al., 2004b). Progressive shear wetting would result in a more constant flow velocity, and hence a more uniform distribution of the deposit (De Blasio et al., 2005).

3.1.3 Liquefaction

We follow Ogata et al., (2014) in invoking liquefaction as a possible mechanism to explain the mobility of MTDs. Liquefaction involves the transformation of sediments from a solid-like state into a fluid-like state (Allen, 1982; Maltman and Bolton, 2003; Owen, 1987). According to Ogata et al., (2014) the relationship between shear zones and liquefaction in undrained, poorly-consolidated sediments is a major component in controlling flow mobility by promoting the reduction of basal and internal frictional forces. These authors invoke liquefaction of fine-grained sediments throughout the mass flow to account for their mobility. However, we propose a specific mechanism involving the liquefaction of poorly-packed sand immediately below the sea floor over which the mass flow is moving (Ogata et al., 2012). During shear induced by the over-riding flow, the framework of grain contacts within the sand is lost, producing a quasi-Newtonian low viscosity layer immediately below the mass flow. The liquefied sand bed thus acts as a virtually friction-free shear zone at the sea floor. As the flow finally comes to rest, the liquefied sand injects upwards into the basal part of the MTD (**Fig 2b**).

Hydroplaning, shear wetting and liquefaction are thus three, possibly concomitant mechanisms for the formation of a lubricating layer at the base of a mass flow. They result in the loss of shear strength at the base of the flow, and the prevention of shear stress transmission from the flow into the substrate due to the difference in viscosity.

Nevertheless, even though the shear wetting process has been observed in experiments, the process is not yet fully understood and there are many uncertainties regarding sediment behaviour (De Blasio and Elverhøi, 2011; De Blasio et al., 2005). Hydroplaning on the otherhand is well documented and understood in laboratory examples (e.g. Ilstad et al., 2004a; Mohrig et al., 1999, 1998). However, there is to date no evidence of hydroplaning or shear wetting flows in nature, although liquefaction is well documented in MTDs from outcrop studies (e.g. Lowe, 1976; Odonne et al., 2011; Ogata et al., 2014; Owen, 1996; Strachan, 2002; Talling et al., 2013).

3.2 No-slip flows

We employ the term ‘no-slip flows’ to refer to mass flows with a zero- or limited-slip boundary with the substrate, which thus interact significantly with the sea floor (for example where they erode or deform it). No-slip flows may produce a spectrum of interactions ranging

from sole marks through substantial erosion to substrate deformation that penetrates to significant depths below the base of the displaced mass (**Fig 2c and d**).

3.2.1 Substrate erosion

Submarine MTDs containing large blocks are commonly observed in modern and ancient deepwater sedimentary basins (e.g. Alves, 2015; Dunlap et al., 2010; Jackson, 2011; Macdonald et al., 1993). These blocks can be divided into either autochthonous or allochthonous blocks. Autochtonous or remnant blocks are interpreted as *in situ* masses of sediment that have not experienced failure and translation (e.g. Bull et al., 2009) and are still connected to the unremobilized substrate. On the other hand allochthonous or rafted blocks are coherent bodies of sediment that are carried within the MTD, therefore do not possess any sort of connection with the substrate. Such blocks can originate either by disaggregation of the failed MTD protolith, or by interaction between the MTD and the substrate through basal erosion. Nevertheless, care must be taken when identifying their origin since blocks may originate by erosion close to their initial failure, and thus possess the same lithology as the MTD matrix; also MTDs may have a heterogeneous composition reflecting a range of lithologies at the point of failure (e.g. Festa et al., 2016; Macdonald et al., 1993; Sobiesiak et al., 2016b), which could lead to misinterpretation. Distinction of block and matrix lithologies(and thus identification of block origin) may not be possible in seismic data. Nonetheless, when analysing the seismic expression of MTD´s blocks from offshore Morocco, Lee et al., (2004) observed velocity sags beneath many of the blocks and suggested that this decrease in velocity could be lithology related, suggesting that differentiation of block lithology in seismic may be possible in some circumstances.

The presence of a heterogeneous block assemblage within MTDs suggests that the flow may have interacted with the substrate at some point. Although the results of this interaction (typically small-scale) can locally be seen in outcrop (e.g. Butler and McCaffrey, 2010; Dakin et al., 2013; Dykstra et al., 2011; Ogata et al., 2012; Sobiesiak et al., 2016a) the true nature and geometry of the erosion are best appreciated in seismic data. In the case of no-slip flows, this means that the shear stress at the base of the flow is transmitted to the substrate without being moderated by the presence of any lubricating layer (see above). Since the contrast in material properties between the flow and substrate is likely to be relatively small compared to free-slip flows, shear stress can be effectively transmitted across the flow´s lower boundary. Three scenarios can be expected as a consequence of shear stress

transmission; **(i)** substrate material is sheared off (eroded) and incorporated into the flow (**Fig 2c**); **(ii)** substrate becomes internally deformed through plastic deformation (**Fig 2d**); and **(iii)** a mixture of both. The features resulting from seafloor erosion described in the literature are many. However, we propose a simplified and comprehensive classification for such features using their geometry as a parameter to define; **(i)** megascours and scours (**Fig 3**), **(ii)** grooves (**Fig 5**) and **(iii)** peel-back scours (**Fig 7**).

3.2.1.1 Megascours and scours

The term megascour was coined by Moscardelli et al., (2006) to define a ~60 kilometre long erosional feature, ranging from 2 to 7 kilometres in width and up to 33 metres deep developed at the base of a submarine MTD offshore Trinidad and Venezuela (**Fig 4a**). Subsequently, megascour has been used to describe any large-scale erosional feature. In this study, megascours and scours are both classified as a generic erosional features with no pre-defined shape, that may contain other types of erosion within, and which may occur across a variety of scales from outcrop to seismic and are, therefore, the largest features described here (**Fig 3**).

Such features are recognized in outcrop; Dakin et al., (2013) described two examples of what they referred to as megascours preserved in the Middle Eocene Ainsa Basin in Spain, though these features are on a slightly smaller scale than those described by Moscardelli et al. (2006). One of the scours is ~25 metres wide and ~12 metres deep and the other is a concave-up shaped scour up to ~1 kilometre wide and 35 metres deep (**Fig 4b**). Dykstra et al., (2011) and Sobiesiak et al., (2016b) also described an extremely irregular basal boundary (**Fig 4c**) from a ~180 metres thick Carboniferous mass transport deposit (here termed MTDII) located at Cerro Bola mountain in NW Argentina. The basal irregularity displays cuspate-shaped scours that reach up to hundreds of metres in length and ~20 metres in depth. Furthermore, both outcrop examples contain disaggregated floating sandstone blocks interpreted by the authors as derived from the erosion of the semi- or unconsolidated underlying sandstone, suggesting the basal scours resulted from the translation of one or several erosive MTDs over the sandy substrate (Dakin et al., 2013; Dykstra et al., 2011; Milana et al., 2010; Sobiesiak et al., 2016a). Additional seismic scale examples from Moscardelli et al., (2006) highlight the variability in scale of these structures and form an erosional escarpment (~70 kilometres long, ~10 kilometres wide and ~250 metres deep) that contains the megascour (described above) plus a smaller secondary scour (>1 kilometre wide, extending from 10 to 20 kilometres and less than 20 metres deep) (**Fig 4a**).

228 3.2.1.2 Grooves (tool marks)

229 Another mechanism for local erosion of the substrate is by dragging of tools such as rigid
230 blocks contained at the base of the flow (**Fig 5**). These create linear features on the
231 flow/substrate boundary and can occur as either a single feature or in a bundle. The process
232 of tooling the substrate is a common feature at the base of submarine debris flows, where an
233 object capable of eroding the substrate tends to remain at the base of the debris flow for long
234 periods, until either being disaggregated via friction with the substrate, or lifted off the base
235 of the flow (Posamentier and Martinsen, 2011). We categorise grooves here as linear or
236 slightly sinuous features that are V-shaped in cross section (e.g. Bull et al., 2009; Posamentier
237 and Martinsen, 2011), and are typically narrow and deep in relation to other erosional
238 features described here (**Fig 5**).

239 Posamentier and Kolla, (2003) observed long linear grooved patterns at the base of a
240 mass transport deposit offshore Kalimantan, eastern Borneo. Here the grooves extend up to
241 20 kilometres in length, are over 25 metres wide and 15 metres deep, and have an overall
242 'V'-shape in cross-section. Similar linear features, termed 'furrows' by Gee et al., (2006), are
243 described from offshore Angola, where the furrows are up to ~ 10 kilometres long and ~20
244 metres deep, with an overall 'V' shaped profile. Garyfalou, (2015) also presents a clear
245 example from the Amazon fan, where the basal surface of a shallow sub-surface MTD is
246 dominated updip by the headwall scar and frontal ramp (**Fig 6a)** and by grooves downdip
247 (**Fig 6b**).

248 Grooves are also recorded as small-scale features at outcrop, with Draganits et al., (2008)
249 documenting 4 metres wide, 0.2 metres deep and 35 metres long grooves related to a
250 submarine landslide in the Phe Formation, northwest Himalaya. Dakin et al., (2013) also
251 described small scale grooves made by the friction and dragging of small objects (e.g.
252 pebbles) at the base of an eroding debris flow from the Ainsa System of the Hecho Group,
253 Spanish Pyrenees.

254 3.2.1.3 Peel-back scour

255 Clusters of erosional features that diverge down-flow and display a square-shaped
256 termination are described from offshore Brunei, and have been termed 'monkey fingers' by
257 McGilvery and Cook, (2003) (**Fig 7a**). These authors suggest that this geometry is related to
258 basal gouging followed by the removal of the gouging tool (grooves). However similar
259 features are described as single square-shaped or flat-bottom structures by Gee et al., (2006,

2005) as ‘striations’, by Moscardelli et al., (2006) as ‘cat claws’ and Gamberi et al., (2011) as ‘megascours’. They are suggested to originate by the sliding or dragging of tabular blocks into the substrate (Gamberi et al., 2011; Gee et al., 2005) or by the transitional state of flow confinement (Moscardelli et al., 2006).

We propose here that these features are the result of peeling back of the substrate (**Fig 7b and c**). As the flow moves over the basal detachment, the shear stress is transmitted into the uppermost few- or tens- of metres of the substrate, pushing and/or peeling the sediments in the flow direction. Where a weak layer is present, the substrate detaches along this horizon and is translated in a manner analogous to a thrust sheet, creating a negative feature within the substrate, which displays a box-shaped geometry in cross section, bounded laterally by sub-vertical strike-slip shear zones. The failed material is pushed in the transport direction and is buttressed against a frontal ramp where the detachment ramps up to the sea floor, or to a shallower detachment surface. In such cases, either an imbricate thrust system develops (**Fig 7c, d**) or the scour is completely evacuated and the material is disaggregated and incorporated into the moving flow. Peel-back features are usually wide and shallow with a characteristic flat-bottom.

All types of erosional features described above can be used as kinematic indicators for the movement of MTDs, as the linear axis of scours, grooves and/or peel-backs are usually parallel or elongated towards the main flow direction (e.g. Bull et al., 2009; Butler et al., 2016; Butler and Tavarnelli, 2006; Ogata et al., 2016; Sobiesiak, 2016). The differentiation of MTD erosional features from turbidite erosion can be inferred on the basis of their occurrence upslope and/or beneath blocky debris flows (e.g. grooves and megascours) and/or beyond the downslope termination of a mass flow (e.g. glide track) (Bull et al., 2009; Gee et al., 2005).

3.2.2 Substrate deformation

When a submarine mass flow moves downslope it translates over a detachment surface (BSS). This surface is developed due to progressive shear failure and defines the terminus or the base of the MTD, thus separating deformed, chaotic and disrupted strata from continuous strata of the undeformed substrate or coherent deposits down-dip (e.g.Bull et al., 2009; Frey-Martínez et al., 2006; Hampton et al., 1996; Omosanya and Alves, 2013). However, the basal shear surface may be complex, and localised deformation has been described in the substrate (e.g. Alves, 2015; Laberg et al., 2016; Ogata et al., 2012; Sobiesiak et al., 2016a). This results in folds and other deformational features that attenuate downwards from the slide surface

(Alves, 2015; Alves and Lourenço, 2010). These deformation structures are the result of stress penetration into the substrate, commonly due to localised variation in the basal shear surface geometry (e.g.ramp and flat system) (**Fig 1b**) affected by faults, bedding planes or material property variation (Alves and Lourenço, 2010; Bull et al., 2009; Omosanya and Alves, 2013).

Alves and Lourenço, (2010) consider palaeo-seafloor deformation from outcrops of a submarine landslide in SE Crete, where the authors analysed the deformation underneath rafted megablocks. The deformation was recorded through the first few metres below the basal contact of the megablocks, with a sharp change into undeformed strata. A similar observation was made by Alves, (2015) from seismic data from offshore SE Brazil, revealing the complexity of the basal shear surface, where the reflectors show a thick continuous deformed zone between the MTD and the surface that is normally mapped as the basal shear surface (see Fig. 08a from Alves, (2015)). Such observations indicate that the basal shear surface can be more than a simple surface separating deformed from undeformed strata, and therefore the basal boundary is a shear zone rather than a single shear surface (Alves, 2015; Alves and Lourenço, 2010).

Based on these observations of basal deformation (**Fig 2d**), and on an outcrop case study from the Guandacol Formation (Carboniferous) in Cerro Bola, NW Argentina, we propose two basic types of basal deformation, termed continuous no-slip and discontinuous no-slip (**Fig 8a and b**).

3.2.2.1 Basal Shear Zone

The Argentinian case study consists of two seismic-scale MTDs intercalated with sandstone packages related to deltaic progradation. The stratigraphy of the interval of interest comprise roughly 500 metres of sedimentary rocks, encompassing a fluvio-deltaic succession (FDI), overlain by an MTD (MTD I), another fluvio-deltaic succession (FD II), followed by the upper MTD (MTD II) and ending in ponded turbidite sandstones (e.g. Milana et al., 2010).The upper MTD (MTD II) is up to ~180 metres thick, and contains characteristically large, relatively undeformed exotic sandstone blocks, which are preserved throughout the whole deposit (Sobiesiak et al., 2016b). The sandstone blocks are typically larger and more abundant towards the MTD base, where they comprise up to ~30% of the deposit by volume. These blocks are interpreted to be derived from the underlying sandstone substrate, from which they were eroded and incorporated into the flow during transport. This process resulted

in local erosional features such as scours along the basal contact (described above in Section 3.2.1.1), and soft sediment deformation that affects the uppermost ~20 metres of the underlying sandstones (Sobiesiak et al., 2016a). Deformation in the contact with substrate commences at the MTD and continues downward to a sharp shear surface that defines the boundary between deformed and undeformed sandstones (**Fig. 8a and 9b**)

The sections containing deformed strata throughout the whole ~20 metres are defined as continuous no-slip (**Fig. 8a and 9b**). Some sections, however, are virtually undeformed within the first couple of metres of sandstone, followed by ~ 18 metres of deformed strata; these sections are here termed discontinuous no-slip (**Fig. 8b and 9a**). In both cases, the deformation is recorded as a series of soft sediment structures such as recumbent, overturned, parasitic (S and Z) fold types (**Fig. 9c**), boulder rotation (**Fig. 9d**), boudins, pinch and swell structures (**Fig. 9e**), mullion structures (**Fig. 9f**), bed attenuation and the formation of proto-block shaped structures (which are similar in shape to the entrained blocks within the overlain MTD) (**Fig. 9a and b**). Additionally the outcrop displays deformation and shearing of thin sand layers, that vary in thickness from a couple of millimetres up to ~5 centimetres (**Fig. 9g**). Similar deformation and shearing of sand layers are documented adjacent to the sandstone blocks in the overlying MTD (see Sobiesiak et al., 2016b).

The main difference between continuous and discontinuous no-slip basal deformation is that in the latter case, the uppermost few of metres of substrate sandstone are undeformed (**Fig. 9a**). One interpretation for such conservation is that the yield strength of the uppermost few metres is higher than the underlying strata, and that the slab was thus welded to the base of the mass movement with zero or limited slip. The underlying strata served as a weak layer over which the undeformed slab slipped with little or no internal strain. These sections are characterised by the preservation of primary structures such as right way-up sets of planar cross-stratification and trough cross-bedding (**Fig. 9a and 10a**). The undeformed sandstone is limited at the upper boundary by the base of the debris flow and at the lower boundary by a shear surface.

The distribution of fold hinges from the deformed sandstone interval is shown in stereonets (**Fig. 10b**). The folds were categorised into east-verging folds (blue dots) and west-verging folds (red dots). The east-verging folds are marked by NW-dipping axial planes (mean strike and dip 205°/65°NW), while the west-verging folds have E-dipping axial planes (mean strike and dip 036°/45°SE). Both east and west-verging folds display SSW plunging

hinges (mean 208°) with hinge trends distributed over a 154° arc. The distribution of fold hinges and their scattered pattern suggest that the deformation was dominated by layer parallel shear (Alsop et al., 2016; Alsop and Holdsworth, 2007), meaning that fold hinges and associated axial planes originated at right angles to the downslope/transport direction. Furthermore, there is no indication of fold hinge and axial plane rotation towards the transport direction during progressive deformation. Application of the mean axial method (MAM of Alsop and Marco, (2012) indicates an overall transport orientation of 298°, which corroborates previously published assessments by Milana et al., (2010), Dykstra et al., (2011) and Sobiesiak et al., (2016b) that indicate transport towards the NW or WNW.

Another example from Cerro Bola is the basal shear zone developed between the lower MTD (MTD I) and the underlying sandstone (FD I) described by Valdez et al., (2015). The characteristics of the MTD are very similar to the one described above, namely a ~115 metres thick debris flow including large-scale sandstone blocks, interpreted to originate by the interaction between the MTD and the substrate. A ~14 metres thick deformation zone (basal shear zone) can be seen in the uppermost part of the underlying sandstone (**Fig. 10c**). The zone includes highly deformed sediments containing pinch and swell structures along with folding in a highly sheared matrix. According to the Valdez et al. (2015) the deformation style resembles ductile structures described in metamorphic rocks.

The total thickness (~20m) of the basal shear zone described from below the younger Argentinian MTD (MTD II) is ~11% of the total thickness of the overlying deposit (~180m), while the thickness (~14m) of the basal shear zone below the older Argentinian MTD (MTD I) is ~12%. Together with data published by Alves and Lourenço (2010) demonstrating the thickness of the deformed material is ~15% the thickness of the overlying slide blocks (Alves, 2015), these observations corroborate the interpretation that occasionally the basal surface may consist of a shear zone rather than a simple detachment surface. Alves and Lourenço (2010) pointed out that a change in the physical properties of the substrate in response to submarine debris flow may be enough to cause the deformation zone described above. Moreover, the following variables may be sufficient to influence the occurrence, style, and thickness of the deformation zone; (i) whether the substrate consists of an older debris flow rather than a well layered sequence; (ii) MTD velocity and thickness; (iii) presence and distribution of weak layers that can dissipate shear stress and cause a reduction in the basal shear zone thickness; (iv) physical state and properties of the substrate sediments (lithified or

unlithified, density, thickness); (v) nature of the mass flow (slide, slump, debris flow) and style (confined and unconfined); among others (Alves and Lourenço, 2010).

4 Conclusion

A broad classification is proposed here (free- and no-slip flows) to decribe the styles of basal interaction beneath submarine mass movements. We discuss three mechanisms for substrate erosion and two types for substrate deformation. The principal conclusions of this work can be summarised as follows:

Free-slip flows

(i) Hydroplaning, shear wetting and liquefaction act as potential mechanisms that allow mass movements to detach from the substrate. This leads to flow bypass (**Fig 2a and b**), prevents shear stress transmission into the substrate, and thereby limits any potential erosion or deformation.

No-slip flows

(ii) Megascours and scours(**Fig 3**) are erosional mechanisms where the basal drag is great enough to allow the mass movement to plough into the substrate, thereby pulling and/or ripping up the substrate and incorporating it into the moving flow. Grooves (**Fig 5**) result from the dragging of a tool carried at the base of the flow that is pressed against the substrate, and leaves a scour-shaped track of its passage. Finally, peel-back (**Fig 7**) is developed when the substrate is pushed by the flow along a basal detachement (weak layer) laterally bounded by sub-vertical strike-slip shear zones, resulting in a flat- bottomed box-shaped erosional feature.

(iii) Continuous and discontinuous no-slip basal deformation (**Fig 8**) describes the situation where the strain front related to the mass movement does not coincide with the base of the mass flow but occurs a considerable depth into the substrate, resulting in the development of a basal shear zone (**Fig 11**).

5 Acknowledgments

We acknowledge the support of CNPq (Conselho Nacional de Desenvolvimento Científico e Tecnológico) - Brazil, Shell and the University of Aberdeen. The authors would like to thank GCSSEPM and SEPM for permission to publish some of their published figures

and to all authors whose works were cited here as case studies.We would like to thank the following colleagues for their support, camaraderie and countless hours of fieldwork: Claus Fallgatter, Victoria Valdez, Carla Puigdomenech, Guilherme Bozetti, Roberto Noll Filho, Arthur Lemos Giovannini, Qun Liu, Thisiane dos Santos, Pan Li, Amanda Santa Catarina, Ramon Lopez Jimenez and Larissa Hansen. Last but not least, we thank Lorena Moscardelli and Kei Ogata for their insightful reviews that improved this manuscript

6 References

Allen, J.R.L., 1982. Sedimentary Structures: Their Character and Physical Basis.

Alsop, G.I., Holdsworth, R.E., 2007. Flow perturbation folding in shear zones. Geol. Soc. London, Spec. Publ. 272, 75–101. https://doi.org/10.1144/GSL.SP.2007.272.01.06

Alsop, G.I., Marco, S., 2012. A large-scale radial pattern of seismogenic slumping towards the Dead Sea Basin. J. Geol. Soc. London. 169, 99–110. https://doi.org/10.1144/0016-76492011-032

Alsop, G.I., Marco, S., Weinberger, R., Levi, T., 2016. Sedimentary and structural controls on seismogenic slumping within mass transport deposits from the Dead Sea Basin. Sediment. Geol. 344, 71–90. https://doi.org/10.1016/j.sedgeo.2016.02.019

Alves, T.M., 2015. Submarine slide blocks and associated soft-sediment deformation in deep-water basins: A review. Mar. Pet. Geol. 67, 262–285. https://doi.org/10.1016/j.marpetgeo.2015.05.010

Alves, T.M., Lourenço, S.D.N.N., 2010. Geomorphologic features related to gravitational collapse: Submarine landsliding to lateral spreading on a Late Miocene–Quaternary slope (SE Crete, eastern Mediterranean). Geomorphology 123, 13–33. https://doi.org/10.1016/j.geomorph.2010.04.030

Alves, T.M., Strasser, M., Moore, G.F.F., 2013. Erosional features as indicators of thrust fault activity (Nankai Trough, Japan). Mar. Geol. 356, 5–18. https://doi.org/10.1016/j.margeo.2013.07.011

Bull, S., Cartwright, J., Huuse, M., 2009. A review of kinematic indicators from mass-transport complexes using 3D seismic data. Mar. Pet. Geol. 26, 1132–1151. https://doi.org/10.1016/j.marpetgeo.2008.09.011

Butler, R.W.H., Eggenhuisen, J.T., Haughton, P., McCaffrey, W.D., 2016. Interpreting syndepositional sediment remobilization and deformation beneath submarine gravity flows; a kinematic boundary layer approach. J. Geol. Soc. London. 173, 46–58. https://doi.org/10.1144/jgs2014-150

Butler, R.W.H., McCaffrey, W.D., 2010. Structural evolution and sediment entrainment in mass-transport complexes: outcrop studies from Italy. J. Geol. Soc. London. 167, 617–

631. https://doi.org/10.1144/0016-76492009-041

Butler, R.W.H., Tavarnelli, E., 2006. The structure and kinematics of substrate entrainment into high-concentration sandy turbidites: a field example from the Gorgoglione “flysch” of southern Italy. Sedimentology 53, 655–670. https://doi.org/10.1111/j.1365-3091.2006.00789.x

Dakin, N., Pickering, K.T., Mohrig, D., Bayliss, N.J., 2013. Channel-like features created by erosive submarine debris flows: Field evidence from the Middle Eocene Ainsa Basin, Spanish Pyrenees. Mar. Pet. Geol. 41, 62–71. https://doi.org/10.1016/j.marpetgeo.2012.07.007

De Blasio, F. V., Elverhøi, A., 2011. Properties of mass-transport deposits as inferred from dynamic modeling of subaqueous mass wasting: A short review. Mass-transport Depos. Deep. Settings 499–508. https://doi.org/De Blasio, F. V., Elverhøi, A., 2011. Properties of mass-transport deposits as inferred from dynamic modeling of subaqueous mass wasting: A short review. Mass-transport Depos. Deep. Settings 499–508.

De Blasio, F.V.F. V., Elverhøi, A., Issler, D., Harbitz, C.B., Bryn, P., Lien, R., 2005. On the dynamics of subaqueous clay rich gravity mass flows—the giant Storegga slide, Norway. Mar. Pet. Geol. 22, 179–186. https://doi.org/10.1016/j.marpetgeo.2004.10.014

Denne, R.A., Scott, E.D., Eickhoff, D.P., Kaiser, J.S., Hill, R.J., Spaw, J.M., 2013. Massive Cretaceous-Paleogene boundary deposit, deep-water Gulf of Mexico: New evidence for widespread Chicxulub-induced slope failure. Geology 41, 983–986. https://doi.org/10.1130/G34503.1

Dott, R.H., 1963. Dynamics of subaqueous gravity depositional processes. Bull. Am. Assoc. Pet. Geol. 47, 104–128.

Draganits, E., Schlaf, J., Grasemann, B., Argles, T., 2008. Giant submarine landslide grooves in the Neoproterozoic/Lower Cambrian Phe Formation, northwest Himalaya: Mechanisms of formation and palaeogeographic implications. Sediment. Geol. 205, 126–141. https://doi.org/10.1016/j.sedgeo.2008.02.004

Dunlap, D.B., Wood, L.J., Weisenberger, C., Jabour, H., 2010. Seismic geomorphohgy of offshore Morocco’s east margin, Safi Haute Mer area. Am. Assoc. Pet. Geol. Bull. 94, 615–642. https://doi.org/10.1306/10270909055

Dykstra, M., Garyfalou, K., Kertznus, V., Kneller, B., Milana, J.P., Milinaro, M., Szuman, M., Thompson, P., 2011. Mass-Transport Deposits: Combining outcrop studies and seismic forward modeling to understand lithofacies distributions, deformation, and their seismic expression. SEPM Spec. Publ. 95, 1–25.

Elverhøi, A., Issler, D., De Blasio, F. V., Ilstad, T., Harbitz, C.B., Gauer, P., 2005. Emerging insights into the dynamics of submarine debris flows. Nat. Hazards Earth Syst. Sci. 5, 633–648. https://doi.org/10.5194/nhess-5-633-2005

Festa, A., Ogata, K., Pini, G.A., Dilek, Y., Alonso, J.L., 2016. Origin and significance of olistostromes in the evolution of orogenic belts: A global synthesis. Gondwana Res. 39, 180–203. https://doi.org/10.1016/j.gr.2016.08.002

Frey-Martínez, J., Cartwright, J., James, D., 2006. Frontally confined versus frontally emergent submarine landslides: A 3D seismic characterisation. Mar. Pet. Geol. 23, 585–604. https://doi.org/http://dx.doi.org/10.1016/j.marpetgeo.2006.04.002

Gamberi, F., Rovere, M., Marani, M., 2011. Mass-transport complex evolution in a tectonically active margin (Gioia Basin, Southeastern Tyrrhenian Sea). Mar. Geol. 279, 98–110. https://doi.org/10.1016/j.margeo.2010.10.015

Garyfalou, K., 2015. Integrated analysis of mass-transport deposits: Outcrop, 3D seismic interpretation and fast fourier transform. Unpublished PhD thesis, University of Aberdeen.

Gawthorpe, R.L., Clemmey, H., 1985. Geometry of submarine slides in the Bowland Basin (Dinantian) and their relation to debris flows. J. Geol. Soc. London. 142, 555–565. https://doi.org/10.1144/gsjgs.142.3.0555

Gee, M.J.R., Gawthorpe, R.L., Friedmann, J.S., 2005. Giant striations at the base of a submarine landslide. Mar. Geol. 214, 287–294. https://doi.org/10.1016/j.margeo.2004.09.003

Gee, M.J.R., Gawthorpe, R.L., Friedmann, S.J., 2006. Triggering and Evolution of a Giant Submarine Landslide, Offshore Angola, Revealed by 3D Seismic Stratigraphy and Geomorphology. J. Sediment. Res. 76, 9–19. https://doi.org/10.2110/jsr.2006.02

Gee, M.J.R., Masson, D.G., Watts, A.B., Allen, P.A., 1999. The Saharan debris flow: an insight into the mechanics of long runout submarine debris flows. Sedimentology 46,

317–335. https://doi.org/10.1046/j.1365-3091.1999.00215.x

Hampton, M.A., Lee, H.J., Locat, J., 1996. Submarine landslides. Rev. Geophys. 34, 33–59. https://doi.org/10.1029/95RG03287

Ilstad, T., De Blasio, F. V., Elverhøi, A., Harbitz, C.B., Engvik, L., Longva, O., Marr, J.G., 2004a. On the frontal dynamics and morphology of submarine debris flows. Mar. Geol. 213, 481–497. https://doi.org/10.1016/j.margeo.2004.10.020

Ilstad, T., Elverhøi, A., Issler, D., Marr, J.G., 2004b. Subaqueous debris flow behaviour and its dependence on the sand/clay ratio: a laboratory study using particle tracking. Mar. Geol. 213, 415–438. https://doi.org/10.1016/j.margeo.2004.10.017

Jackson, C. a.-L., 2011. Three-dimensional seismic analysis of megaclast deformation within a mass transport deposit; implications for debris flow kinematics. Geology 39, 203–206. https://doi.org/10.1130/G31767.1

Kneller, B., Dykstra, M., Fairweather, L., Milana, J.P., 2016. Mass-transport and slope accommodation: Implications for turbidite sandstone reservoirs. Am. Assoc. Pet. Geol. Bull. 100, 213–235. https://doi.org/10.1306/09011514210

Laberg, J.S., Strasser, M., Alves, T.M., Gao, S., Kawamura, K., Kopf, A., Moore, G.F., 2016. Internal deformation of a muddy gravity flow and its interaction with the seafloor (site C0018 of IODP Expedition 333, Nankai Trough, SE Japan). Landslides 14, 849–860. https://doi.org/10.1007/s10346-016-0766-7

Lee, H., Normark, W., Fisher, M., Greene, H., Edwards, B., Locat, J., 2004. Timing and Extent of Submarine Landslides in Southern California, in: Proceedings of Offshore Technology Conference. The Offshore Technology Conference. https://doi.org/10.4043/16744-MS

Lowe, D.R., 1976. Subaqueous liquefied and fluidized sediment flows and their deposits. Sedimentology 23, 285–308. https://doi.org/10.1111/j.1365-3091.1976.tb00051.x

Lucente, C.C., Pini, G.A., 2003. Anatomy and emplacement mechanism of a large submarine slide within a Miocene foredeep in the northern Apennines, Italy: a field perspective. Am. J. Sci. 303, 565–602.

Macdonald, D.I.M., Moncrieff, A.C.M., Butterworth, P.J., 1993. Giant slide deposits from a Mesozoic fore-arc basin, Alexander Island, Antarctica. Geology 21, 1047.

https://doi.org/10.1130/0091-7613(1993)021<1047:GSDFAM>2.3.CO;2

Maltman, A.J., Bolton, A., 2003. How sediments become mobilized. Subsurf. Sediment Mobilization 216, 9–20. https://doi.org/10.1144/GSL.SP.2003.216.01.02

McGilvery, T.A. (Mac), Cook, D.L., 2003. The Influence of Local Gradients on Accommodation Space and Linked Depositional Elements Across a Stepped Slope Profile, Offshore Brunei, in: Shelf Margin Deltas and Linked Down Slope Petroleum Systems: 23rd Annual. SOCIETY OF ECONOMIC PALEONTOLOGISTS AND MINERALOGISTS, pp. 387–419. https://doi.org/10.5724/gcs.03.23.0387

Middleton, G. V, Hampton, M.A., 1973. Sediment gravity flows: mechanics of flow and deposition. SEPM Pacific Sect. short course Lect. notes 1–38. https://doi.org/-

Milana, J.P., Kneller, B., Dykstra, M., 2010. Mass-Transport Deposits and Turbidites, Syn-to-Post-Glacial Carboniferous Basins of Western Argentina. ISC 2010 F. Guid. 01–88.

Mohrig, D., Ellis, C., Parker, G., Whipple, K.X., Hondzo, M., 1998. Hydroplaning of subaqueous debris flows. Geol. Soc. Am. Bull. 110, 387–394. https://doi.org/10.1130/0016-7606(1998)110<0387:HOSDF>2.3.CO;2

Mohrig, D., Elverhøi, A., Parker, G., 1999. Experiments on the relative mobility of muddy subaqueous and subaerial debris flows, and their capacity to remobilize antecedent deposits. Mar. Geol. 154, 117–129. https://doi.org/10.1016/S0025-3227(98)00107-8

Moscardelli, L., Wood, L., 2015. Morphometry of mass-transport deposits as a predictive tool. Geol. Soc. Am. Bull. 128, B31221.1. https://doi.org/10.1130/B31221.1

Moscardelli, L., Wood, L., 2008. New classification system for mass transport complexes in offshore Trinidad. Basin Res. 20, 73–98. https://doi.org/10.1111/j.1365-2117.2007.00340.x

Moscardelli, L., Wood, L., Mann, P., 2006. Mass-transport complexes and associated processes in the offshore area of Trinidad and Venezuela. Am. Assoc. Pet. Geol. Bull. 90, 1059–1088. https://doi.org/10.1306/02210605052

Nardin, T.R., Hein, F.J., Gorsline, D.S., Edwards, B.D., 1979. A review of mass movement processes, sediment and acoustic characteristics, and contrasts in slope and base-of-slope systems versus canyon-fan-basin floor systems., in: Geology of Continental Slopes. SEPM (Society for Sedimentary Geology), pp. 61–73.

https://doi.org/10.2110/pec.79.27.0061

Nissen, S.E., Haskell, N.L., Steiner, C.T., Coterill, K.L., 1999. Debris flow outrunner blocks, glide tracks, and pressure ridges identified on the Nigerian continental slope using 3-D seismic coherency. Lead. Edge 18, 595–599. https://doi.org/10.1190/1.1438343

Odonne, F., Callot, P., Debroas, E.-J., Sempere, T., Hoareau, G., Maillard, A., 2011. Soft-sediment deformation from submarine sliding: Favourable conditions and triggering mechanisms in examples from the Eocene Sobrarbe delta (Ainsa, Spanish Pyrenees) and the mid-Cretaceous Ayabacas Formation (Andes of Peru). Sediment. Geol. 235, 234–248. https://doi.org/10.1016/j.sedgeo.2010.09.013

Ogata, K., Mountjoy, J.J., Pini, G.A., Festa, A., Tinterri, R., 2014. Shear zone liquefaction in mass transport deposit emplacement: A multi-scale integration of seismic reflection and outcrop data. Mar. Geol. 356, 50–64. https://doi.org/10.1016/j.margeo.2014.05.001

Ogata, K., Mutti, E., Pini, G.A., Tinterri, R., 2012. Mass transport-related stratal disruption within sedimentary mélanges: Examples from the northern Apennines (Italy) and south-central Pyrenees (Spain). Tectonophysics 568–569, 185–199. https://doi.org/10.1016/j.tecto.2011.08.021

Ogata, K., Pini, G.A., Festa, A., Pogačnik, Ž., Lucente, C.C., 2016. Meso-Scale Kinematic Indicators in Exhumed Mass Transport Deposits: Definitions and Implications, in: Lamarche, G., Mountjoy, J., Bull, S., Hubble, T., Krastel, S., Lane, E., Micallef, A., Moscardelli, L., Mueller, C., Pecher, I., Woelz, S. (Eds.), Submarine Mass Movements and Their Consequences, 7th International Symposium. Advance in Natural and Technological Hazards Research, Springer, The Netherlands., Advances in Natural and Technological Hazards Research. Springer International Publishing, Cham, pp. 461–468. https://doi.org/10.1007/978-3-319-20979-1_46

Omosanya, K.O., Alves, T.M., 2013. Ramps and flats of mass-transport deposits (MTDs) as markers of seafloor strain on the flanks of rising diapirs (Espírito Santo Basin, SE Brazil). Mar. Geol. 340, 82–97. https://doi.org/10.1016/j.margeo.2013.04.013

Owen, G., 1996. Experimental soft-sediment deformation: structures formed by the liquefaction of unconsolidated sands and some ancient examples. Sedimentology 43, 279–293. https://doi.org/10.1046/j.1365-3091.1996.d01-5.x

603 Owen, G., 1987. Deformation processes in unconsolidated sands. Geol. Soc. London, Spec.
604 Publ. 29, 11–24. https://doi.org/10.1144/GSL.SP.1987.029.01.02

605 Posamentier, H.W., Kolla, V., 2003. Seismic Geomorphology and Stratigraphy of
606 Depositional Elements in Deep-Water Settings. J. Sediment. Res. 73, 367–388.
607 https://doi.org/10.1306/111302730367

608 Posamentier, H.W., Martinsen, O.J., 2011. The Character and Genesis of Submarine Mass-
609 Transport Deposits: Insights from Outcrop and 3D Seismic Data, in: Mass-Transport
610 Deposits in Deepwater Settings. SEPM (Society for Sedimentary Geology), pp. 7–38.
611 https://doi.org/10.2110/sepmsp.096.007

612 Posamentier, H.W., Walker, R.G., 2006. Deep-Water Turbidites and Submarine Fans, in:
613 Facies Models Revisited. SEPM (Society for Sedimentary Geology), pp. 399–520.

614 Prior, D.B., Bornhold, B.D., Johns, M.W., Suhayda, J.N., Bornhold, B.D., Johns, M.W.,
615 1984. Depositional characteristcs of a submarine debris flow. J. Geol. 92, 707–727.
616 https://doi.org/00221376

617 Sobiesiak, M.S., 2016. Failure, kinematics and strain distribution in Mass Transport Deposits
618 (MTDs) and the interaction with the substrate. Unpublished PhD thesis, University of
619 Aberdeen.

620 Sobiesiak, M.S., Kneller, B., Alsop, G.I., Milana, J.P., 2016a. Inclusion of Substrate Blocks
621 Within a Mass Transport Deposit: A Case Study from Cerro Bola, Argentina, in:
622 Lamarche, G., Mountjoy, J., Bull, S., Hubble, T., Krastel, S., Lane, E., Micallef, A.,
623 Moscardelli, L., Mueller, C., Pecher, I., Woelz, S. (Eds.), Submarine Mass Movements
624 and Their Consequences, 7th International Symposium. Advance in Natural and
625 Technological Hazards Research, Springer, The Netherlands., Advances in Natural and
626 Technological Hazards Research. Springer International Publishing, Cham, pp. 487–
627 496. https://doi.org/10.1007/978-3-319-20979-1_49

628 Sobiesiak, M.S., Kneller, B., Alsop, G.I., Milana, J.P., 2016b. Internal deformation and
629 kinematic indicators within a tripartite mass transport deposit, NW Argentina. Sediment.
630 Geol. 344, 364–381. https://doi.org/10.1016/j.sedgeo.2016.04.006

631 Strachan, L.J., 2002. Slump-initiated and controlled syndepositional sandstone
632 remobilization: An example from the Namurian of county Clare, Ireland. Sedimentology

633 49, 25–41. https://doi.org/10.1046/j.1365-3091.2002.00430.x

634 Talling, P.J., Malgesini, G., Felletti, F., 2013. Can liquefied debris flows deposit clean sand
635 over large areas of sea floor? Field evidence from the Marnoso-arenacea Formation,
636 Italian Apennines. Sedimentology 60, 720–762. https://doi.org/10.1111/j.1365-
637 3091.2012.01358.x

638 Toniolo, H., Harff, P., Marr, J.G., Paola, C., Parker, G., 2004. Experiments on Reworking by
639 Successive Unconfined Subaqueous and Subaerial Muddy Debris Flows. J. Hydraul.
640 Eng. 130, 38–48. https://doi.org/10.1061/(ASCE)0733-9429(2004)130:1(38)

641 Valdez, V.B., Milana, J.P., Kneller, B.C., 2015. Megadeslizamientos gravitacionales de la
642 formación guandacol en Cerro Bola y Sierra de Maz y su relación con la glaciación del
643 Paleozoico tardío, La Rioja, Argentina. Lat. Am. J. Sedimentol. Basin Anal. 22, 109–
644 133.

645

646 Allen, J.R.L., 1982. Sedimentary Structures: Their Character and Physical Basis.

647 Alsop, G.I., Holdsworth, R.E., 2007. Flow perturbation folding in shear zones. Geol. Soc.
648 London, Spec. Publ. 272, 75–101. https://doi.org/10.1144/GSL.SP.2007.272.01.06

649 Alsop, G.I., Marco, S., 2012. A large-scale radial pattern of seismogenic slumping towards
650 the Dead Sea Basin. J. Geol. Soc. London. 169, 99–110. https://doi.org/10.1144/0016-
651 76492011-032

652 Alsop, G.I., Marco, S., Weinberger, R., Levi, T., 2016. Sedimentary and structural controls
653 on seismogenic slumping within mass transport deposits from the Dead Sea Basin.
654 Sediment. Geol. 344, 71–90. https://doi.org/10.1016/j.sedgeo.2016.02.019

655 Alves, T.M., 2015. Submarine slide blocks and associated soft-sediment deformation in deep-
656 water basins: A review. Mar. Pet. Geol. 67, 262–285.
657 https://doi.org/10.1016/j.marpetgeo.2015.05.010

658 Alves, T.M., Lourenço, S.D.N.N., 2010. Geomorphologic features related to gravitational
659 collapse: Submarine landsliding to lateral spreading on a Late Miocene–Quaternary
660 slope (SE Crete, eastern Mediterranean). Geomorphology 123, 13–33.
661 https://doi.org/10.1016/j.geomorph.2010.04.030

662 Alves, T.M., Strasser, M., Moore, G.F.F., 2013. Erosional features as indicators of thrust fault
663 activity (Nankai Trough, Japan). Mar. Geol. 356, 5–18.
664 https://doi.org/10.1016/j.margeo.2013.07.011

665 Bull, S., Cartwright, J., Huuse, M., 2009. A review of kinematic indicators from mass-
666 transport complexes using 3D seismic data. Mar. Pet. Geol. 26, 1132–1151.
667 https://doi.org/10.1016/j.marpetgeo.2008.09.011

668 Butler, R.W.H., Eggenhuisen, J.T., Haughton, P., McCaffrey, W.D., 2016. Interpreting
669 syndepositional sediment remobilization and deformation beneath submarine gravity
670 flows; a kinematic boundary layer approach. J. Geol. Soc. London. 173, 46–58.
671 https://doi.org/10.1144/jgs2014-150

672 Butler, R.W.H., McCaffrey, W.D., 2010. Structural evolution and sediment entrainment in
673 mass-transport complexes: outcrop studies from Italy. J. Geol. Soc. London. 167, 617–
674 631. https://doi.org/10.1144/0016-76492009-041

675 Butler, R.W.H., Tavarnelli, E., 2006. The structure and kinematics of substrate entrainment
676 into high-concentration sandy turbidites: a field example from the Gorgoglione “flysch”
677 of southern Italy. Sedimentology 53, 655–670. https://doi.org/10.1111/j.1365-
678 3091.2006.00789.x

679 Dakin, N., Pickering, K.T., Mohrig, D., Bayliss, N.J., 2013. Channel-like features created by
680 erosive submarine debris flows: Field evidence from the Middle Eocene Ainsa Basin,
681 Spanish Pyrenees. Mar. Pet. Geol. 41, 62–71.
682 https://doi.org/10.1016/j.marpetgeo.2012.07.007

683 De Blasio, F. V., Elverhøi, A., 2011. Properties of mass-transport deposits as inferred from
684 dynamic modeling of subaqueous mass wasting: A short review. Mass-transport Depos.
685 Deep. Settings 499–508. https://doi.org/De Blasio, F. V., Elverhøi, A., 2011. Properties
686 of mass-transport deposits as inferred from dynamic modeling of subaqueous mass
687 wasting: A short review. Mass-transport Depos. Deep. Settings 499–508.

688 De Blasio, F.V.F. V., Elverhøi, A., Issler, D., Harbitz, C.B., Bryn, P., Lien, R., 2005. On the
689 dynamics of subaqueous clay rich gravity mass flows—the giant Storegga slide,
690 Norway. Mar. Pet. Geol. 22, 179–186. https://doi.org/10.1016/j.marpetgeo.2004.10.014

691 Denne, R.A., Scott, E.D., Eickhoff, D.P., Kaiser, J.S., Hill, R.J., Spaw, J.M., 2013. Massive

692 Cretaceous-Paleogene boundary deposit, deep-water Gulf of Mexico: New evidence for
693 widespread Chicxulub-induced slope failure. Geology 41, 983–986.
694 https://doi.org/10.1130/G34503.1

695 Dott, R.H., 1963. Dynamics of subaqueous gravity depositional processes. Bull. Am. Assoc.
696 Pet. Geol. 47, 104–128.

697 Draganits, E., Schlaf, J., Grasemann, B., Argles, T., 2008. Giant submarine landslide grooves
698 in the Neoproterozoic/Lower Cambrian Phe Formation, northwest Himalaya:
699 Mechanisms of formation and palaeogeographic implications. Sediment. Geol. 205,
700 126–141. https://doi.org/10.1016/j.sedgeo.2008.02.004

701 Dunlap, D.B., Wood, L.J., Weisenberger, C., Jabour, H., 2010. Seismic geomorphohgy of
702 offshore Morocco's east margin, Safi Haute Mer area. Am. Assoc. Pet. Geol. Bull. 94,
703 615–642. https://doi.org/10.1306/10270909055

704 Dykstra, M., Garyfalou, K., Kertznus, V., Kneller, B., Milana, J.P., Milinaro, M., Szuman,
705 M., Thompson, P., 2011. Mass-Transport Deposits: Combining outcrop studies and
706 seismic forward modeling to understand lithofacies distributions, deformation, and their
707 seismic expression. SEPM Spec. Publ. 95, 1–25.

708 Elverhøi, A., Issler, D., De Blasio, F. V., Ilstad, T., Harbitz, C.B., Gauer, P., 2005. Emerging
709 insights into the dynamics of submarine debris flows. Nat. Hazards Earth Syst. Sci. 5,
710 633–648. https://doi.org/10.5194/nhess-5-633-2005

711 Festa, A., Ogata, K., Pini, G.A., Dilek, Y., Alonso, J.L., 2016. Origin and significance of
712 olistostromes in the evolution of orogenic belts: A global synthesis. Gondwana Res. 39,
713 180–203. https://doi.org/10.1016/j.gr.2016.08.002

714 Frey-Martínez, J., Cartwright, J., James, D., 2006. Frontally confined versus frontally
715 emergent submarine landslides: A 3D seismic characterisation. Mar. Pet. Geol. 23, 585–
716 604. https://doi.org/http://dx.doi.org/10.1016/j.marpetgeo.2006.04.002

717 Gamberi, F., Rovere, M., Marani, M., 2011. Mass-transport complex evolution in a
718 tectonically active margin (Gioia Basin, Southeastern Tyrrhenian Sea). Mar. Geol. 279,
719 98–110. https://doi.org/10.1016/j.margeo.2010.10.015

720 Garyfalou, K., 2015. Integrated analysis of mass-transport deposits: Outcrop, 3D seismic
721 interpretation and fast fourier transform. Unpublished PhD thesis, University of

722 Aberdeen.

723 Gawthorpe, R.L., Clemmey, H., 1985. Geometry of submarine slides in the Bowland Basin
724 (Dinantian) and their relation to debris flows. J. Geol. Soc. London. 142, 555–565.
725 https://doi.org/10.1144/gsjgs.142.3.0555

726 Gee, M.J.R., Gawthorpe, R.L., Friedmann, J.S., 2005. Giant striations at the base of a
727 submarine landslide. Mar. Geol. 214, 287–294.
728 https://doi.org/10.1016/j.margeo.2004.09.003

729 Gee, M.J.R., Gawthorpe, R.L., Friedmann, S.J., 2006. Triggering and Evolution of a Giant
730 Submarine Landslide, Offshore Angola, Revealed by 3D Seismic Stratigraphy and
731 Geomorphology. J. Sediment. Res. 76, 9–19. https://doi.org/10.2110/jsr.2006.02

732 Gee, M.J.R., Masson, D.G., Watts, A.B., Allen, P.A., 1999. The Saharan debris flow: an
733 insight into the mechanics of long runout submarine debris flows. Sedimentology 46,
734 317–335. https://doi.org/10.1046/j.1365-3091.1999.00215.x

735 Hampton, M.A., Lee, H.J., Locat, J., 1996. Submarine landslides. Rev. Geophys. 34, 33–59.
736 https://doi.org/10.1029/95RG03287

737 Ilstad, T., De Blasio, F. V., Elverhøi, A., Harbitz, C.B., Engvik, L., Longva, O., Marr, J.G.,
738 2004a. On the frontal dynamics and morphology of submarine debris flows. Mar. Geol.
739 213, 481–497. https://doi.org/10.1016/j.margeo.2004.10.020

740 Ilstad, T., Elverhøi, A., Issler, D., Marr, J.G., 2004b. Subaqueous debris flow behaviour and
741 its dependence on the sand/clay ratio: a laboratory study using particle tracking. Mar.
742 Geol. 213, 415–438. https://doi.org/10.1016/j.margeo.2004.10.017

743 Jackson, C. a.-L., 2011. Three-dimensional seismic analysis of megaclast deformation within
744 a mass transport deposit; implications for debris flow kinematics. Geology 39, 203–206.
745 https://doi.org/10.1130/G31767.1

746 Kneller, B., Dykstra, M., Fairweather, L., Milana, J.P., 2016. Mass-transport and slope
747 accommodation: Implications for turbidite sandstone reservoirs. Am. Assoc. Pet. Geol.
748 Bull. 100, 213–235. https://doi.org/10.1306/09011514210

749 Laberg, J.S., Strasser, M., Alves, T.M., Gao, S., Kawamura, K., Kopf, A., Moore, G.F., 2016.
750 Internal deformation of a muddy gravity flow and its interaction with the seafloor (site
751 C0018 of IODP Expedition 333, Nankai Trough, SE Japan). Landslides 14, 849–860.

752 https://doi.org/10.1007/s10346-016-0766-7

753 Lee, H., Normark, W., Fisher, M., Greene, H., Edwards, B., Locat, J., 2004. Timing and
754 Extent of Submarine Landslides in Southern California, in: Proceedings of Offshore
755 Technology Conference. The Offshore Technology Conference.
756 https://doi.org/10.4043/16744-MS

757 Lowe, D.R., 1976. Subaqueous liquefied and fluidized sediment flows and their deposits.
758 Sedimentology 23, 285–308. https://doi.org/10.1111/j.1365-3091.1976.tb00051.x

759 Lucente, C.C., Pini, G.A., 2003. Anatomy and emplacement mechanism of a large submarine
760 slide within a Miocene foredeep in the northern Apennines, Italy: a field perspective.
761 Am. J. Sci. 303, 565–602.

762 Macdonald, D.I.M., Moncrieff, A.C.M., Butterworth, P.J., 1993. Giant slide deposits from a
763 Mesozoic fore-arc basin, Alexander Island, Antarctica. Geology 21, 1047.
764 https://doi.org/10.1130/0091-7613(1993)021<1047:GSDFAM>2.3.CO;2

765 Maltman, A.J., Bolton, A., 2003. How sediments become mobilized. Subsurf. Sediment
766 Mobilization 216, 9–20. https://doi.org/10.1144/GSL.SP.2003.216.01.02

767 McGilvery, T.A. (Mac), Cook, D.L., 2003. The Influence of Local Gradients on
768 Accommodation Space and Linked Depositional Elements Across a Stepped Slope
769 Profile, Offshore Brunei, in: Shelf Margin Deltas and Linked Down Slope Petroleum
770 Systems: 23rd Annual. SOCIETY OF ECONOMIC PALEONTOLOGISTS AND
771 MINERALOGISTS, pp. 387–419. https://doi.org/10.5724/gcs.03.23.0387

772 Middleton, G. V, Hampton, M.A., 1973. Sediment gravity flows: mechanics of flow and
773 deposition. SEPM Pacific Sect. short course Lect. notes 1–38. https://doi.org/-

774 Milana, J.P., Kneller, B., Dykstra, M., 2010. Mass-Transport Deposits and Turbidites, Syn-
775 to-Post-Glacial Carboniferous Basins of Western Argentina. ISC 2010 F. Guid. 01–88.

776 Mohrig, D., Ellis, C., Parker, G., Whipple, K.X., Hondzo, M., 1998. Hydroplaning of
777 subaqueous debris flows. Geol. Soc. Am. Bull. 110, 387–394.
778 https://doi.org/10.1130/0016-7606(1998)110<0387:HOSDF>2.3.CO;2

779 Mohrig, D., Elverhøi, A., Parker, G., 1999. Experiments on the relative mobility of muddy
780 subaqueous and subaerial debris flows, and their capacity to remobilize antecedent
781 deposits. Mar. Geol. 154, 117–129. https://doi.org/10.1016/S0025-3227(98)00107-8

782 Moscardelli, L., Wood, L., 2015. Morphometry of mass-transport deposits as a predictive
783 tool. Geol. Soc. Am. Bull. 128, B31221.1. https://doi.org/10.1130/B31221.1

784 Moscardelli, L., Wood, L., 2008. New classification system for mass transport complexes in
785 offshore Trinidad. Basin Res. 20, 73–98. https://doi.org/10.1111/j.1365-
786 2117.2007.00340.x

787 Moscardelli, L., Wood, L., Mann, P., 2006. Mass-transport complexes and associated
788 processes in the offshore area of Trinidad and Venezuela. Am. Assoc. Pet. Geol. Bull.
789 90, 1059–1088. https://doi.org/10.1306/02210605052

790 Nardin, T.R., Hein, F.J., Gorsline, D.S., Edwards, B.D., 1979. A review of mass movement
791 processes, sediment and acoustic characteristics, and contrasts in slope and base-of-slope
792 systems versus canyon-fan-basin floor systems., in: Geology of Continental Slopes.
793 SEPM (Society for Sedimentary Geology), pp. 61–73.
794 https://doi.org/10.2110/pec.79.27.0061

795 Nissen, S.E., Haskell, N.L., Steiner, C.T., Coterill, K.L., 1999. Debris flow outrunner blocks,
796 glide tracks, and pressure ridges identified on the Nigerian continental slope using 3-D
797 seismic coherency. Lead. Edge 18, 595–599. https://doi.org/10.1190/1.1438343

798 Odonne, F., Callot, P., Debroas, E.-J., Sempere, T., Hoareau, G., Maillard, A., 2011. Soft-
799 sediment deformation from submarine sliding: Favourable conditions and triggering
800 mechanisms in examples from the Eocene Sobrarbe delta (Ainsa, Spanish Pyrenees) and
801 the mid-Cretaceous Ayabacas Formation (Andes of Peru). Sediment. Geol. 235, 234–
802 248. https://doi.org/10.1016/j.sedgeo.2010.09.013

803 Ogata, K., Mountjoy, J.J., Pini, G.A., Festa, A., Tinterri, R., 2014. Shear zone liquefaction in
804 mass transport deposit emplacement: A multi-scale integration of seismic reflection and
805 outcrop data. Mar. Geol. 356, 50–64. https://doi.org/10.1016/j.margeo.2014.05.001

806 Ogata, K., Mutti, E., Pini, G.A., Tinterri, R., 2012. Mass transport-related stratal disruption
807 within sedimentary mélanges: Examples from the northern Apennines (Italy) and south-
808 central Pyrenees (Spain). Tectonophysics 568–569, 185–199.
809 https://doi.org/10.1016/j.tecto.2011.08.021

810 Ogata, K., Pini, G.A., Festa, A., Pogačnik, Ž., Lucente, C.C., 2016. Meso-Scale Kinematic
811 Indicators in Exhumed Mass Transport Deposits: Definitions and Implications, in:

Lamarche, G., Mountjoy, J., Bull, S., Hubble, T., Krastel, S., Lane, E., Micallef, A., Moscardelli, L., Mueller, C., Pecher, I., Woelz, S. (Eds.), Submarine Mass Movements and Their Consequences, 7th International Symposium. Advance in Natural and Technological Hazards Research, Springer, The Netherlands., Advances in Natural and Technological Hazards Research. Springer International Publishing, Cham, pp. 461–468. https://doi.org/10.1007/978-3-319-20979-1_46

Omosanya, K.O., Alves, T.M., 2013. Ramps and flats of mass-transport deposits (MTDs) as markers of seafloor strain on the flanks of rising diapirs (Espírito Santo Basin, SE Brazil). Mar. Geol. 340, 82–97. https://doi.org/10.1016/j.margeo.2013.04.013

Owen, G., 1996. Experimental soft-sediment deformation: structures formed by the liquefaction of unconsolidated sands and some ancient examples. Sedimentology 43, 279–293. https://doi.org/10.1046/j.1365-3091.1996.d01-5.x

Owen, G., 1987. Deformation processes in unconsolidated sands. Geol. Soc. London, Spec. Publ. 29, 11–24. https://doi.org/10.1144/GSL.SP.1987.029.01.02

Posamentier, H.W., Kolla, V., 2003. Seismic Geomorphology and Stratigraphy of Depositional Elements in Deep-Water Settings. J. Sediment. Res. 73, 367–388. https://doi.org/10.1306/111302730367

Posamentier, H.W., Martinsen, O.J., 2011. The Character and Genesis of Submarine Mass-Transport Deposits: Insights from Outcrop and 3D Seismic Data, in: Mass-Transport Deposits in Deepwater Settings. SEPM (Society for Sedimentary Geology), pp. 7–38. https://doi.org/10.2110/sepmsp.096.007

Posamentier, H.W., Walker, R.G., 2006. Deep-Water Turbidites and Submarine Fans, in: Facies Models Revisited. SEPM (Society for Sedimentary Geology), pp. 399–520.

Prior, D.B., Bornhold, B.D., Johns, M.W., Suhayda, J.N., Bornhold, B.D., Johns, M.W., 1984. Depositional characteristcs of a submarine debris flow. J. Geol. 92, 707–727. https://doi.org/00221376

Sobiesiak, M.S., 2016. Failure, kinematics and strain distribution in Mass Transport Deposits (MTDs) and the interaction with the substrate. Unpublished PhD thesis, University of Aberdeen.

Sobiesiak, M.S., Kneller, B., Alsop, G.I., Milana, J.P., 2016a. Inclusion of Substrate Blocks

Within a Mass Transport Deposit: A Case Study from Cerro Bola, Argentina, in: Lamarche, G., Mountjoy, J., Bull, S., Hubble, T., Krastel, S., Lane, E., Micallef, A., Moscardelli, L., Mueller, C., Pecher, I., Woelz, S. (Eds.), Submarine Mass Movements and Their Consequences, 7th International Symposium. Advance in Natural and Technological Hazards Research, Springer, The Netherlands., Advances in Natural and Technological Hazards Research. Springer International Publishing, Cham, pp. 487–496. https://doi.org/10.1007/978-3-319-20979-1_49

Sobiesiak, M.S., Kneller, B., Alsop, G.I., Milana, J.P., 2016b. Internal deformation and kinematic indicators within a tripartite mass transport deposit, NW Argentina. Sediment. Geol. 344, 364–381. https://doi.org/10.1016/j.sedgeo.2016.04.006

Strachan, L.J., 2002. Slump-initiated and controlled syndepositional sandstone remobilization: An example from the Namurian of county Clare, Ireland. Sedimentology 49, 25–41. https://doi.org/10.1046/j.1365-3091.2002.00430.x

Talling, P.J., Malgesini, G., Felletti, F., 2013. Can liquefied debris flows deposit clean sand over large areas of sea floor? Field evidence from the Marnoso-arenacea Formation, Italian Apennines. Sedimentology 60, 720–762. https://doi.org/10.1111/j.1365-3091.2012.01358.x

Toniolo, H., Harff, P., Marr, J.G., Paola, C., Parker, G., 2004. Experiments on Reworking by Successive Unconfined Subaqueous and Subaerial Muddy Debris Flows. J. Hydraul. Eng. 130, 38–48. https://doi.org/10.1061/(ASCE)0733-9429(2004)130:1(38)

Valdez, V.B., Milana, J.P., Kneller, B.C., 2015. Megadeslizamientos gravitacionales de la formación guandacol en Cerro Bola y Sierra de Maz y su relación con la glaciación del Paleozoico tardío, La Rioja, Argentina. Lat. Am. J. Sedimentol. Basin Anal. 22, 109–133.

Figures caption

Fig 1: Schematic drawing showing MTD classification according to their frontal emplacement. **(a)** Frontally-confined mass flow develops when the failed mass does not leave the basal shear surface, and the downslope toe is buttressed against the frontal ramp. **(b)** Frontally-emergent mass flow develops when the failed mass ramps up out of the basal shear surface onto the seabed and is free to spread. Red dashed lines mark where sets of imbricate thrusts will develop; blue lines and dashed lines marks where extensional (listric normal) faults are formed. (Modified from Frey-Martínez et al., 2006)

Fig 2: Cartoon showing the main types of free- and no-slip flows. **Free-slip flows**, **(a)** Hydroplaning and shear wetting models showing the emplacement of a lubricant layer between the mass movement and the underlying substrate. Note the necking area behind the flow head is marked by a stretching zone and a the development of cracks at the base of the flow. (Figure inspired by Fig 12 of Ilstad et al., 2004b) . **(b)** Liquefaction model of poorly-packed sands, when liquefied sand work as a lubricating layer to the mass movement. As the flow is deposited, the liquefied sand injects upwards into the basal part of the MTD. **No-slip flows**; **(c)** Basal erosion model displaying the ploughing, erosion and incorporation of the substrate sediments by the overflowing mass movement. **(d)** Substrate deformation model suggesting the strain transmission from the debris flow into the upper zone of the substrate.

Fig 3: Cartoon of a megascour. **(a)** 3D view of a megascour at its downslope end, where the flow ramps up onto the seafloor. Note a smaller-scale erosional feature contained within the megascour. Black arrow indicates flow direction **(b)** Longitudinal section through a megascour, showing the imbrication generated at the frontal ramp. Location of section is shown in (a).

Fig 4: (a) Seismic example showing the basal erosion caused by a mass movement from the near-seafloor offshore Trinidad. The topography is dominated by the erosional escarpment, a box-shaped megascour, together with secondary scours. All three features described are classified as megascours and scours. Displayed surface interpreted by Moscardelli et al., (2006). **(b)** Interpretation based on photomosaic of an outcrop example showing a megascour from the Ainsa Basin (modified from Dakin et al., (2013)). Palaeoflow is away from the observer. **(c)** Oblique aerial photograph looking east at Cerro Bola, showing the erosive boundary between the MTD and the underlying sandstone substrate. Note the sandstone blocks within the MTD.

Fig 5: Cartoon of a groove. **(a)** 3D view of a groove, showing the dragging tool that scoured the seafloor, resulting in a "V" shaped erosional structure. Black arrow indicates flow direction. **(b)** Cross section through a groove, showing the tool at the erosional front between substrate and flow. Location is shown in (a).

Fig 6: Seismic examples from the Amazon fan (based on Garyfalou, 2015). **(a)** Seismic interpretation of the basal surface of a mass movement, showing the three main features of the basal surface, the headwall scar, the frontal ramp and the grooves. (from (Garyfalou, 2015). **(b)** 3D seismic interpretation of the grooved seafloor. (from Garyfalou, 2015).

Fig 7: (a) Seismic interpretation of the basal surface of a debris flow, showing the divergent square-shaped erosion typical of the "monkey fingers". The red arrow indicates the flow direction to the NNW (from McGilvery and Cook, 2003). **(b)** 3D cartoon of a peel-back, showing the flat-bottomed box-shaped scour and how sediments are pushed forward potentially forming a duplex as the base of the MTD ramps up onto the seafloor. Black arrow indicates flow direction. **(c)** Cross section through the peel back scour showing the duplex imbrication on the frontal ramp. **(d)** Cropped figure 155d from Posamentier and Walker, (2006) to illustrate how a set of duplex imbrication look on a seismic dataset.

Fig 8: Cartoon showing the differences between discontinuous and continuous no-slip substrate deformation. **(a)** Continuous no-slip substrate deformation, showing the complete deformation of the substrate down to a diffuse strain front or sharp shear zone that delimits the deformed from the undeformed strata below. **(b)** Discontinuous no-slip substrate deformation, where the first few metres are undeformed and preserved between two shear zones (top and base), while the rest of the substrate is deformed (label D) down to a diffuse strain front or sharp shear zone.

Fig 9: (a) Panoramic view from Cerro Bola in Argentina of a discontinuous no-slip substrate deformation section, showing soft-sediment deformation within the upper tens of metres of the underlying sandstone. Note that the first two metres of sands are undeformed, and are bounded by the MTD above and a shear-surface below. Red dashed lines and arrow mark the shear zone and shear direction, yellow lines mark deformed bedding and define folds that broadly form a footwall syncline to the shear zone. Section is parallel to the MTD transport direction towards NNW. **(b)** Field example of a continuous no-slip substrate from Cerro Bola, showing the deformed sediments separated from the undeformed by a shear surface (red dotted line). Deformation zone is ~20m thick. Interpretative sketch on the lower

left side. Section is parallel to the MTD transport direction towards NNW. **(c)** Field example of a discontinuous no-slip substrate deformation section. Photograph shows details of parasitic folds located at the hinge of a larger recumbent fold. Note thinner and more attenuated beds on the lower limb of the fold. Location is shown in (a). **(d)** Boulder undergoing clockwise rotation within a flowing matrix. Boulder is inclosed within a red sand layer, with smaller folded sand layers on the top right of the picture. Location is shown in (a). **(e)** Boudin and pinch-and-swell structures suggesting ductile attenuation on the lower limb of the footwall syncline. Location is shown in (a). **(f)** Mullion structure parallel to the inferred transport direction. **(g)** Thin sand layers that are sheared and folded. Location is shown in (a).

Fig 10: (a) Detail of the first two metres below the MTD, showing primary bedding and right-way-up cross-stratification suggesting relatively low strains. Location is shown in Fig 10a. **(b)** Stereonet showing the distribution of fold hinges of east (blue) and west (red) verging folds and the mean axial plane. This provides an approximate flow orientation of NW – SE. **(c)** Photograph showing the basal deformation starting at the base of the MTD into the underlying sandstone. Note the highly deformed sediments. (modified from Valdez et al., 2015).

Fig 11: Cartoons showing the shear stress distribution within an MTD and its substrate for the cases of free-slip basal boundaries, continuous and discontinuous no-slip basal boundaries of the MTD. τ_0: shear stress profile within MTD, τ_{0s}: shear stress profile within substrate, τ_c: yield stress profile of substrate material, Z: height. **(a)** Free-slip case, with no deformation of substrate; **(b)** Continuous no-slip case, where the MTD is effectively bonded to weak substrate, and the strain front the marks the deepest level where shear stress exceeds the yield stress and failure occurs in the substrate. The strain front does not therefore coincide with the base of the debris flow, but occurs a considerable distance into the underlying substrate. The profile of shear stress within the substrate (shown here schematically), and thus the depth to which strain extends, depends upon the material properties of the substrate and the basal shear stress of rhe MTD. **(c)** Discontinuous no-slip case, where the MTD is bonded to strong substrate above a weaker layer.

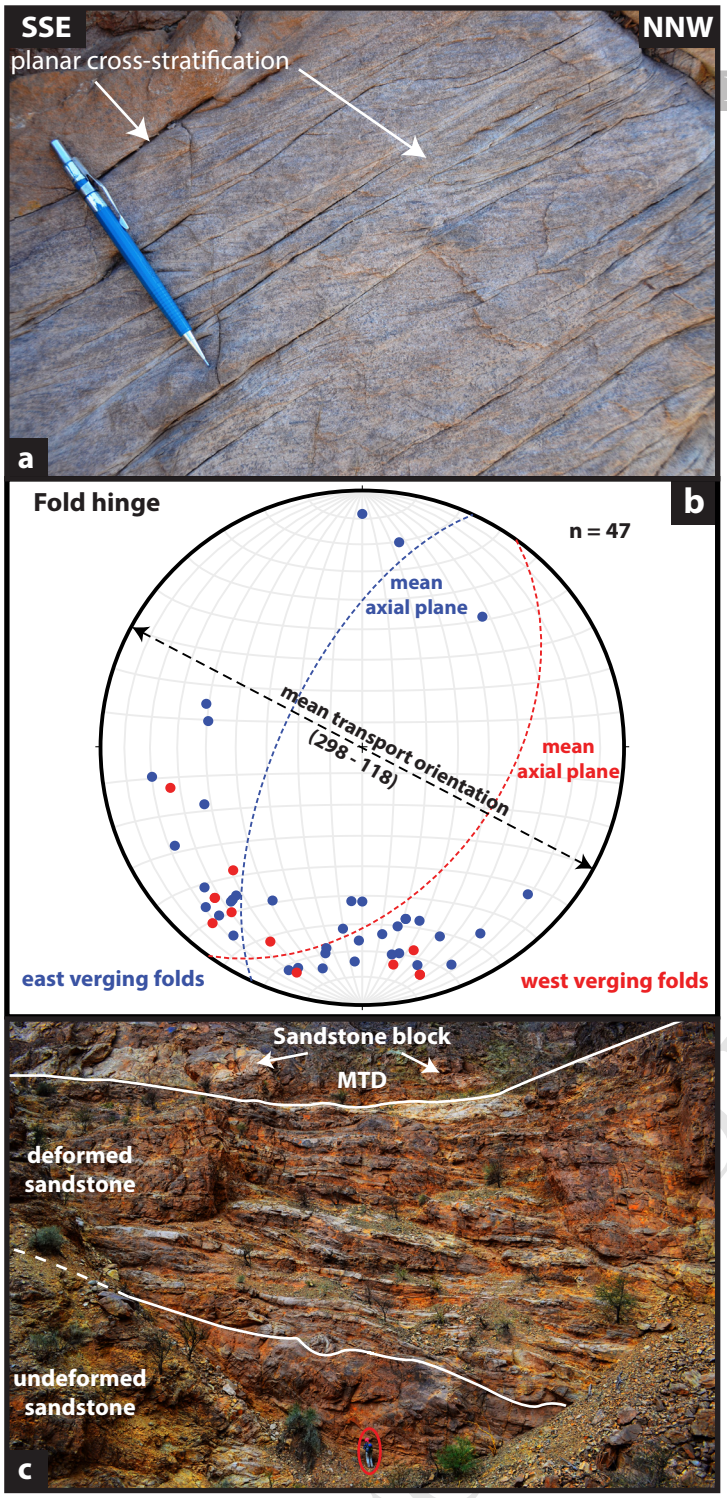

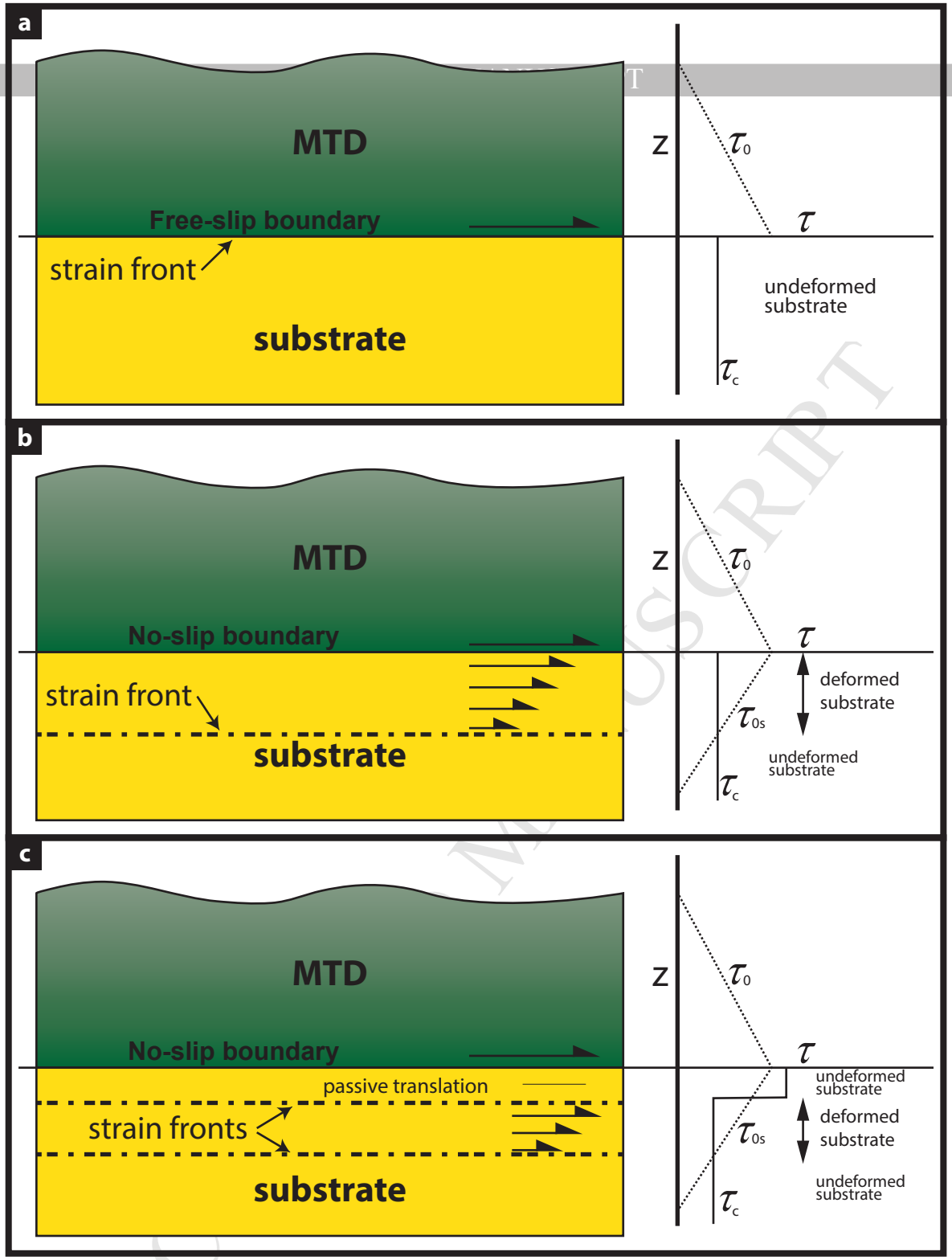
a
MTD
Free-slip boundary
strain front
substrate
z
τ_0
τ
undeformed
substrate
τ_c
b
MTD
No-slip boundary
strain front
substrate
z
τ_0
τ
deformed
substrate
τ_{0s}
undeformed
substrate
τ_c
c
MTD
No-slip boundary
passive translation
strain fronts
substrate
z
τ_0
τ
undeformed
substrate
deformed
substrate
τ_{0s}
undeformed
substrate
τ_c

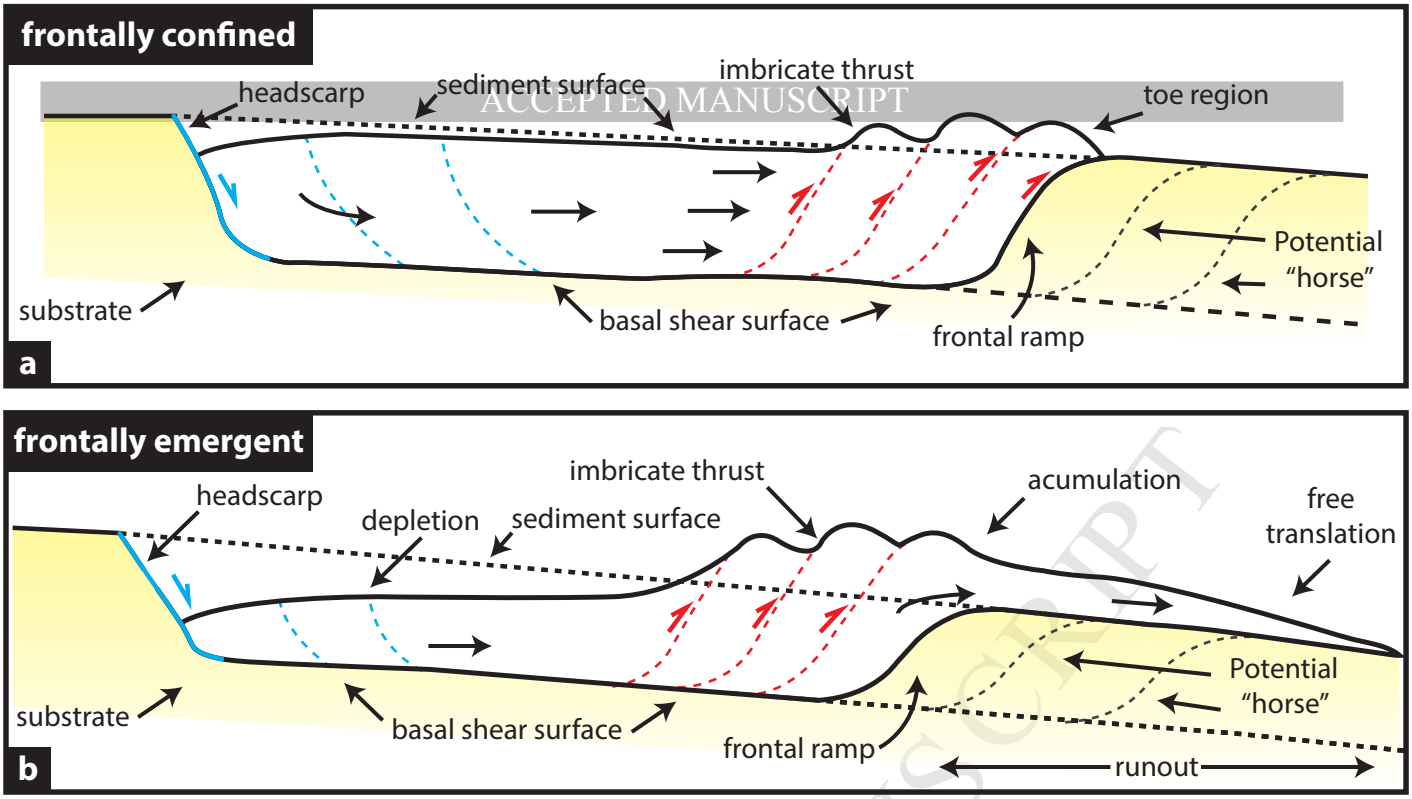

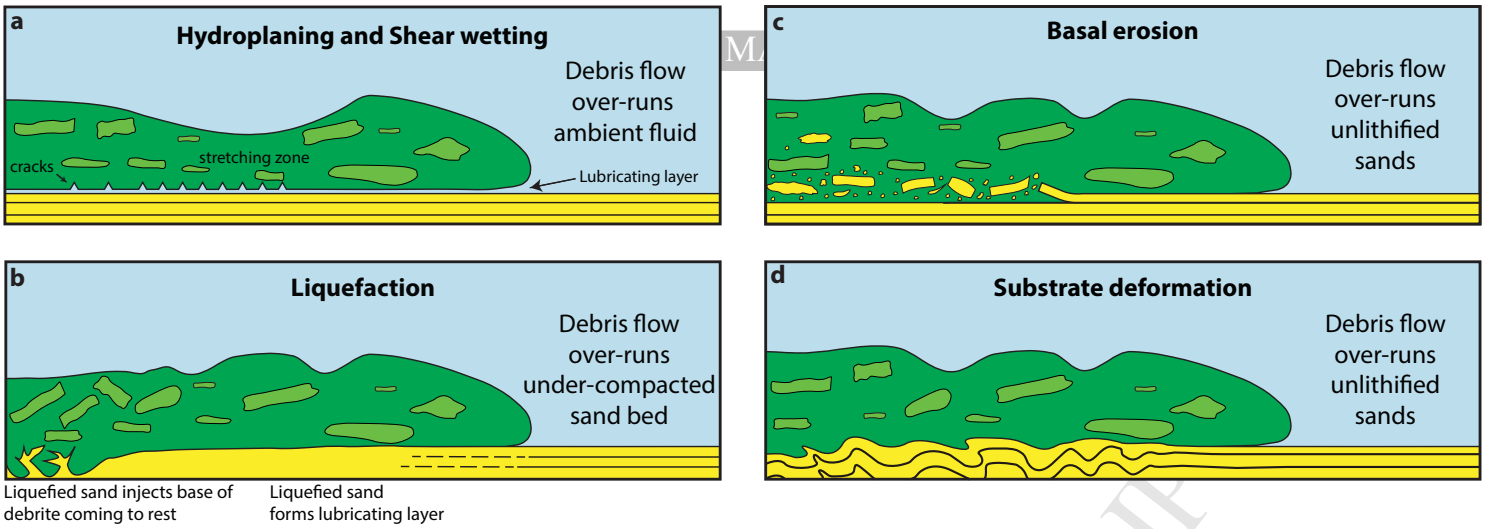

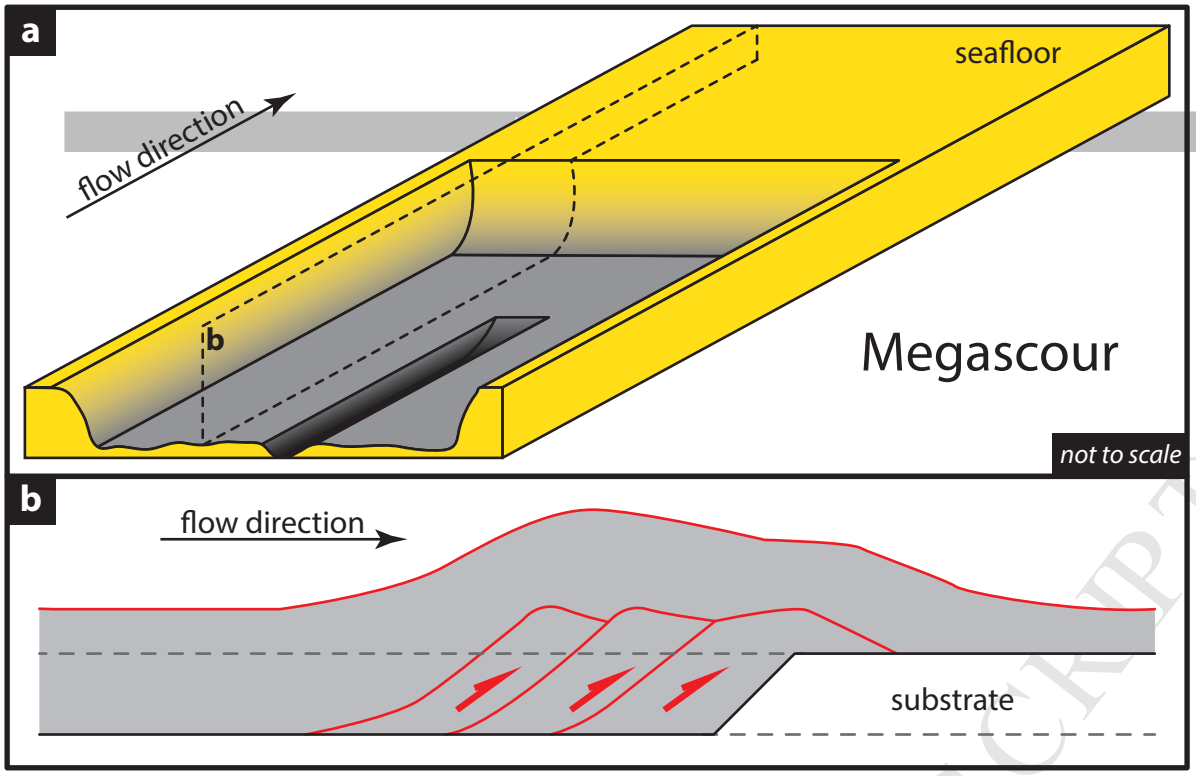

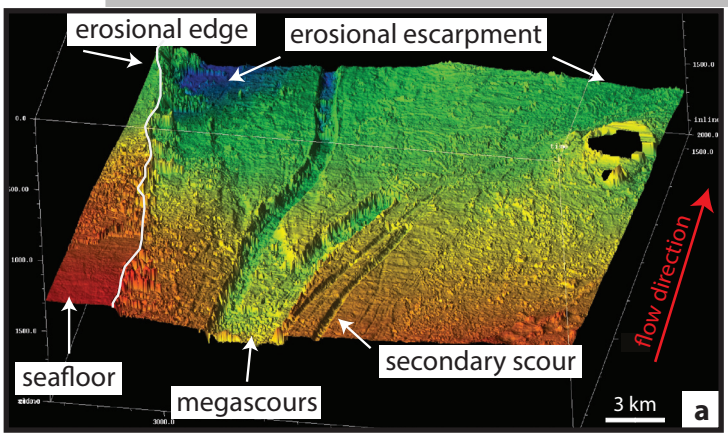

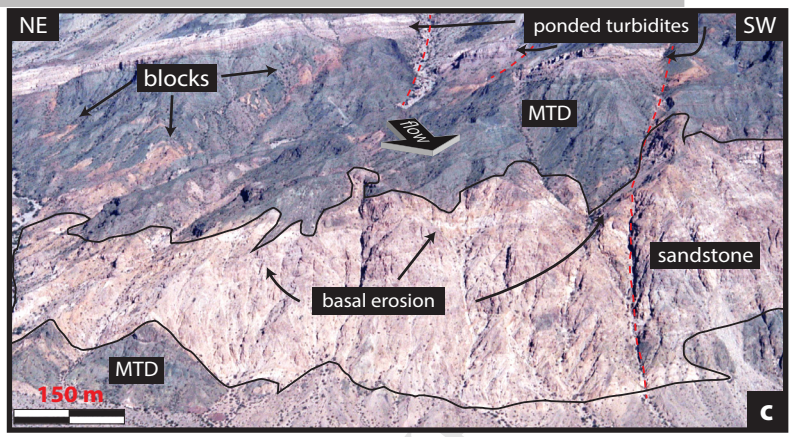

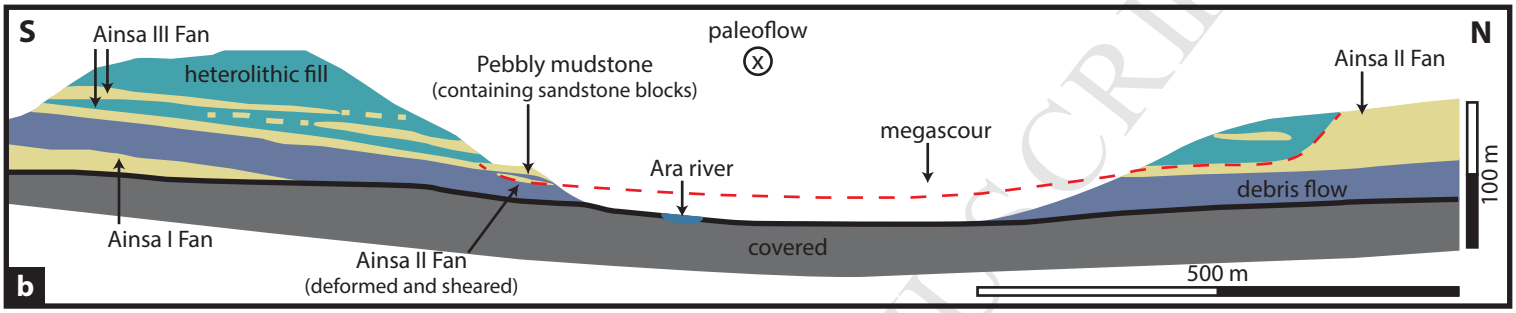

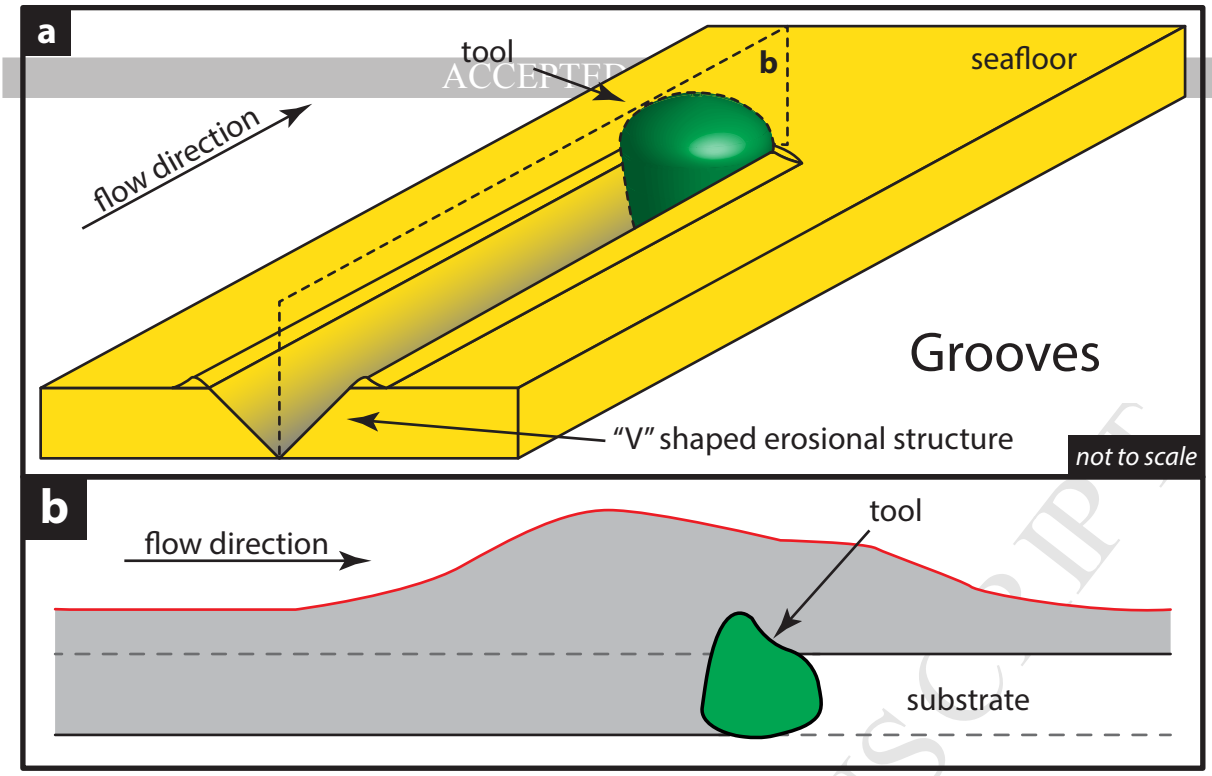

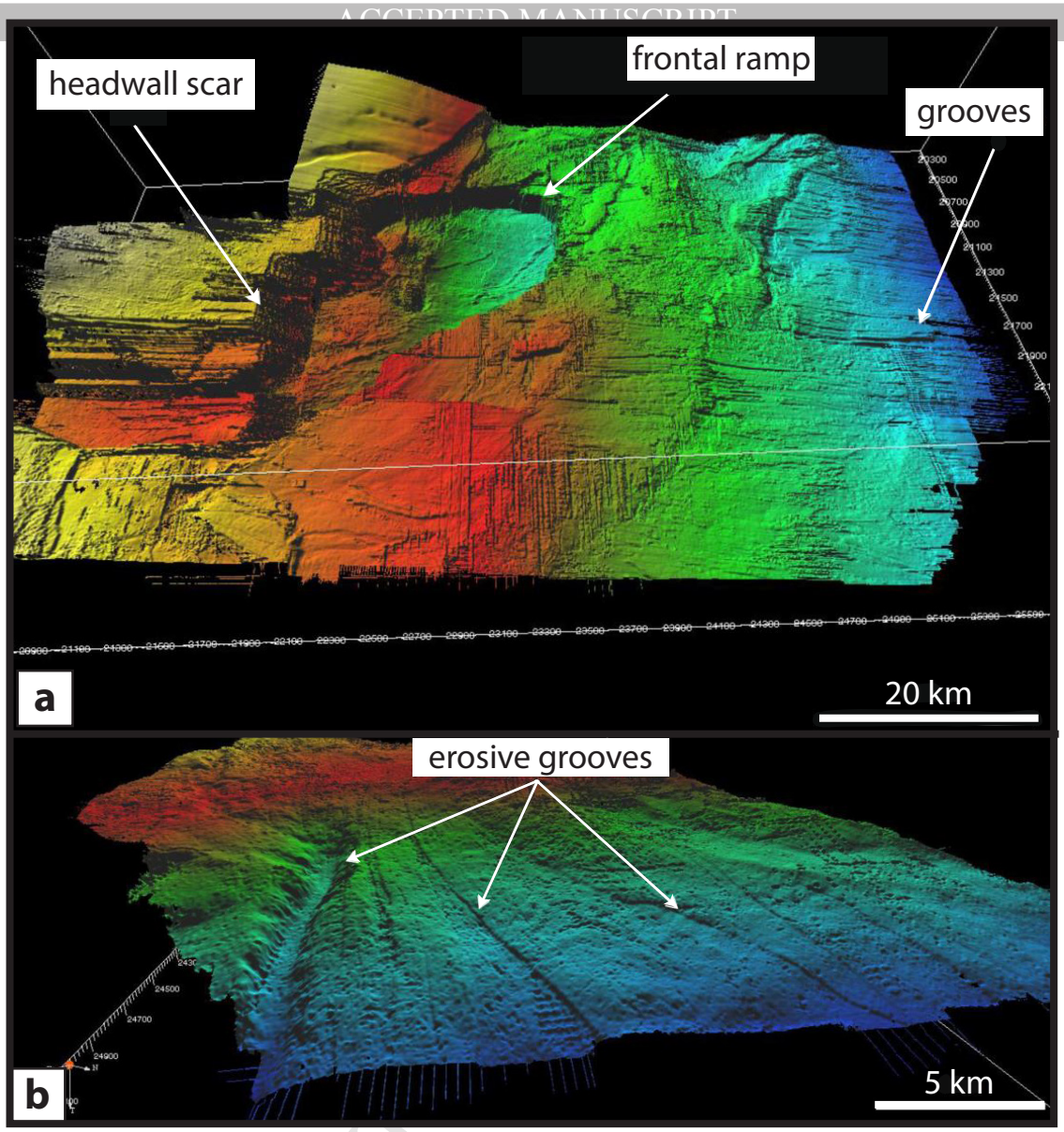

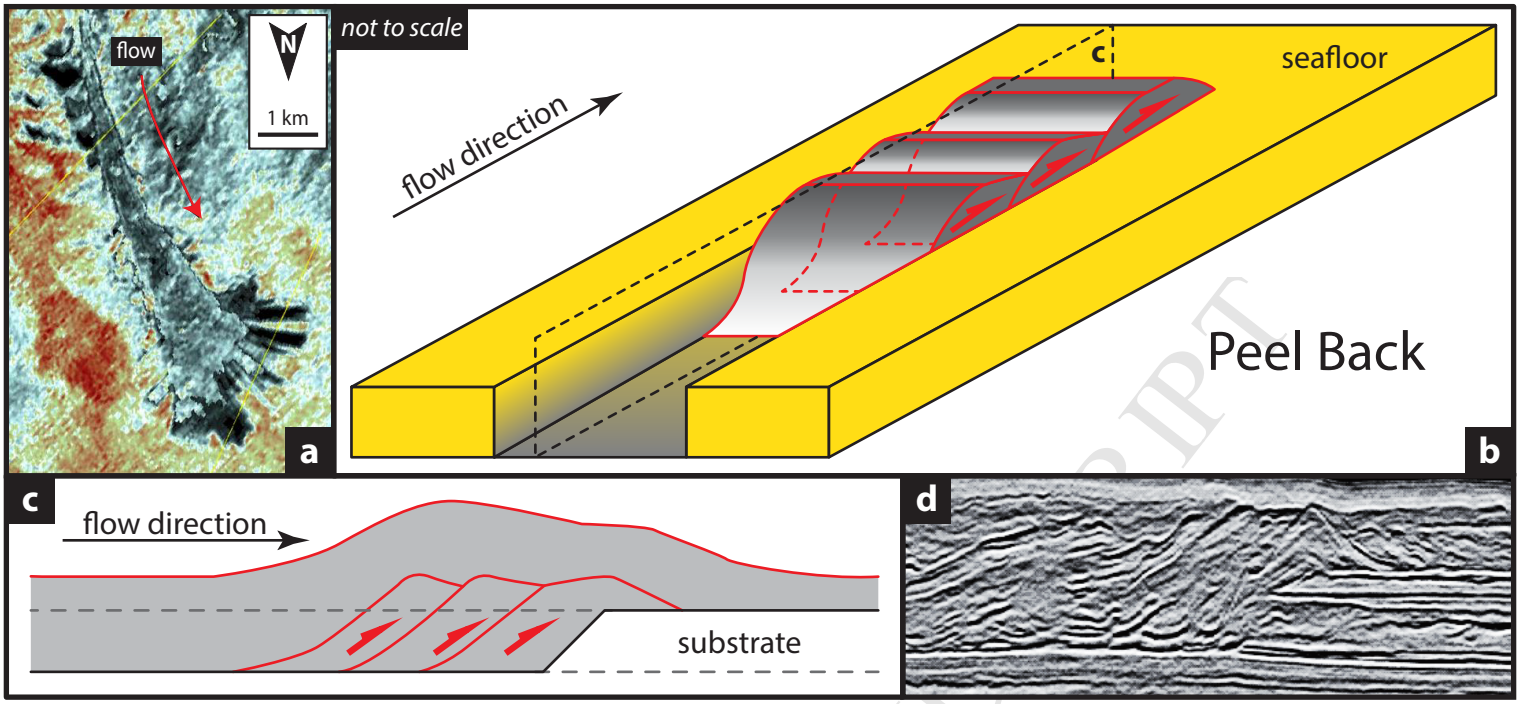

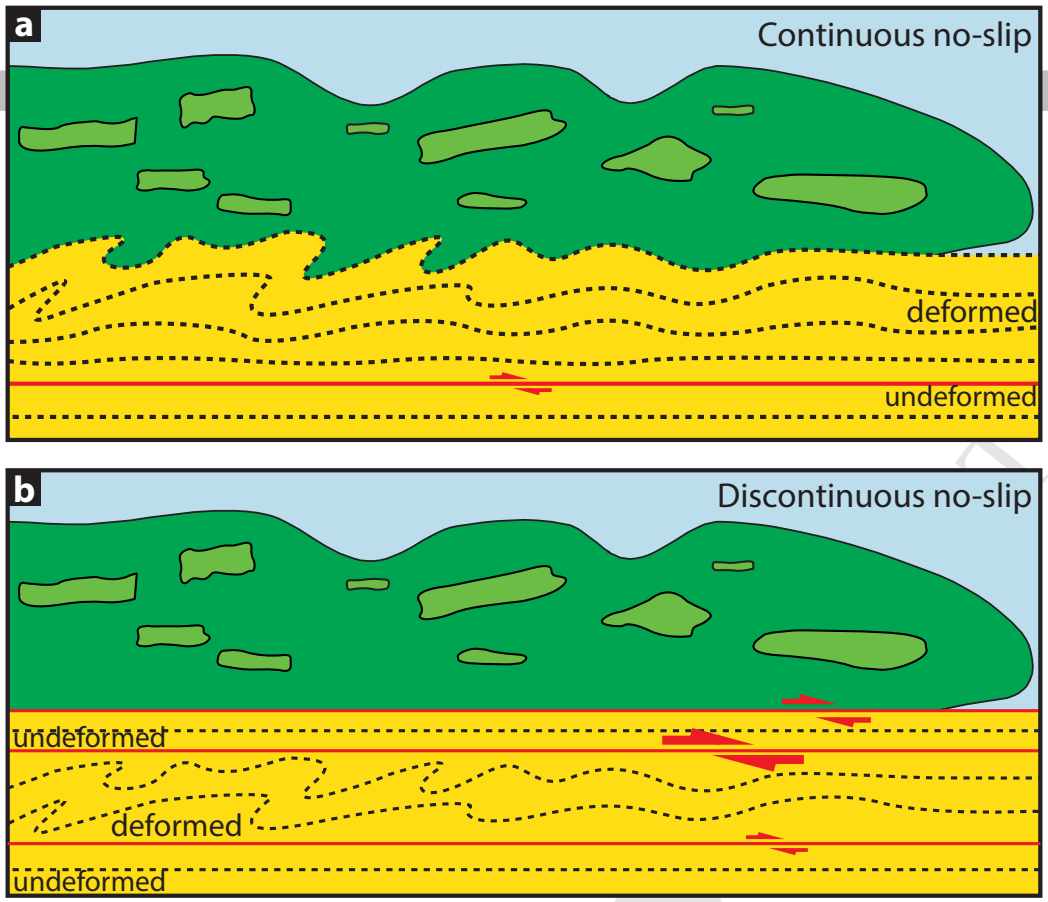


SSE
MTD
undeformed sandstone
deformed sandstone
NNW
10a
c
d
e
g
1m
a
ESE
WNW
block
MTD
deformed sandstone
undeformed sandstone
proto-block
9m
b
SSE
NNW
parasitic fold
recumbent fold
c
SSE
NNW
recumbent fold
bolder
d
SSE
NNW
pinch-and-swell
boudin
e
SSE
NNW
mullion
f
SSE
NNW
sheared and folded sands
g

Highlights

1. Broad classification for basal interaction of submarine mass movements as free- and no-slip flows
2. Hydroplaning, shear wetting and liquefaction are mechanisms resulting in the detachment of the mass flow from the substrate, leading to flow bypass
3. Megascours and peel-back are erosional mechanisms where the basal drag is high enough to allow the mass flow to plough into the substrate.
4. Grooves result from the dragging of a tool carried at the base of the flow.
5. Strain front related to the mass movement does not coincide with the base of the mass flow but may occurs a considerable depth into the substrate.